S04040100-TRT10000-R00

Second Target Station Project: CHESS Technical Report

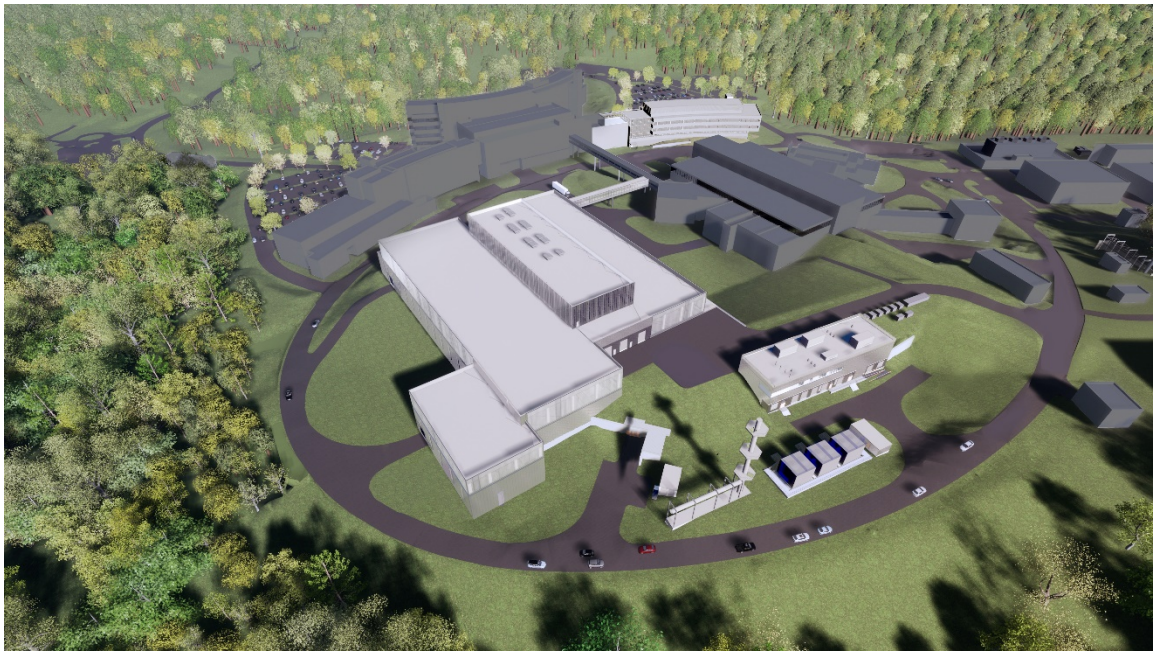

Gabriele Sala
Cristina Boone

July 2023

OAK RIDGE National Laboratory

ORNL IS MANAGED BY UT-BATTELLE LLC FOR THE US DEPARTMENT OF ENERGY

S04040100-TRT10000-R00

Second Target Station Project

CHESS Technical Report

Gabriele Sala
Cristina Boone

July 2023

Prepared by
OAK RIDGE NATIONAL LABORATORY
Oak Ridge, TN 37831
managed by
UT-BATTELLE LLC
for the
US DEPARTMENT OF ENERGY
under contract DE-AC05-00OR22725

Approvals

CHESS Technical Report		ISSUE DATE: July 25, 2023
PREPARED BY Gabriele Sala	PROJECT Second Target Station	DOCUMENT NUMBER: S04040100-TRT10000-R00

	Signature / Date					
	Rev. 00	Date	Rev. 01	Date	Rev. 02	Date
Instrument Systems Lead	Leighton Coates					
Instrument Engineering Manager	Van Graves					
Instr. Sys. Sci. & Technology Manager	Leighton Coates (interim)					
CHESS Lead Scientist	Gabriele Sala					
CHESS Lead Engineer	Cristina Boone					

Revision	Description
00	Initial Release

Table of Figures

List of Acronyms

ALARA	As Low As Reasonably Achievable
ASME	American Society of Mechanical Engineers
CCR	Closed-Cycle Refrigerator
CEC	Credited Engineering Control
CFR	Code of Federal Regulations
CHESS	Chopper spectrometer Examining Small Scatters
CNCS	Cold Neutron Chopper Spectrometer
CW	Chilled Water
DAC	Design Analyses Calculations
DAS	Data Acquisition System
DOE	U.S. Department of Energy
ES&H	Environment, Safety and Health
FSAD	Final Safety Analysis Document
FWHM	Full-Width-at-Half-Maximum
GS	Ground State
HFIR	High Flux Isotope Reactor
HOG	Hot-Off Gas
HVAC	Heating, Ventilation and Air Conditioning
Hz	Hertz (SI physical unit for frequency)
ICS	Instrument Control System
IOC	Input/Output Card
IT	Information Technology
J-PARC	Japan Proton Accelerator Research Complex
KPP	Key Performance Parameter
LPSD	Linear Position Sensitive Detector
McStas	Monte Carlo Simulator for triple axis spectrometer
MCViNE	Monte Carlo Virtual Neutron Experiment
MPS	Machine Protection System
NF	Neutron Facilities
ODH	Oxygen Deficiency Hazard
OLCF	Oak Ridge Leadership Computing Facility
ORNL	Oak Ridge National Laboratory
PF	Proton Facilities
PLC	Programmable Logic Controller
PPS	Personnel Protection System
R&D	Research and Development
RAID	Redundant Array of Inexpensive Disks
RRM	Repetition Rate Multiplication
$S(\boldsymbol{Q},\omega)$	Dynamic scattering function
S&A	Survey and Alignment
SCE	Secondary Confinement Exhaust
SNS	Spallation Neutron Source
STS	Second Target Station
T	Tesla (SI physical unit for magnetic field)
TAS	Triple Axis Spectrometer
K	Kelvin (SI physical unit for temperature)
WBS	Work Breakdown Structure
WSS	Work Smart Standards

ABSTRACT

CHESS is a direct geometry neutron spectrometer designed to detect and analyze weak signals intrinsic to small cross-sections (*e.g.,* small mass, small magnetic moments or neutron absorbing materials). This instrument is optimized to enable unprecedented characterization of quantum materials, spin liquids, thermoelectric and battery materials, liquids, and soft matter. The ability to simultaneously measure dynamic processes over a wide energy range for very small samples will make CHESS the spectrometer of choice for the initial exploration of new materials. The broad dynamic range will also be well matched to measurements of relaxation processes and excitations in soft and biological matter. The 15 Hz repetition rate of STS enables use of multiple incident energies within a single source pulse, greatly expanding the information gained in a single experiment. An essential feature of CHESS is the capability for polarization analysis to separate nuclear from magnetic scattering or coherent from incoherent scattering in hydrogenous materials, and better understanding spin-anisotropic correlations. This instrument will employ advanced sample environments such as high-pressure cells, dilution refrigerators, high field cryo-magnets and polarization devices, as well as combinations of these, to solve problems at the forefront of materials research. CHESS will be one of the flagship spectrometers of the Second Target Station (STS), providing world leading capabilities.

1. SCIENCE CASE

Inelastic neutron scattering (INS) is an essential experimental technique to study the dynamical properties of materials. This technique takes advantage of several fundamental properties of neutrons: the wavelength and energy of neutrons available at neutron sources are well matched to the length and time scales of condensed matter systems; the neutron spin conveys the ability to probe magnetic cross-sections and to polarize beams; the neutron is sensitive to light atoms; the neutron's small cross section allows it to penetrate through complicated sample environments. The measured scattering function $S(\boldsymbol{Q},\omega)$ is proportional to the imaginary part of a generalized momentum and energy-dependent susceptibility, and thus it is straightforward to make a quantitative comparison between experiment and theory. This method provides critical information needed to develop a successful theory for unveiling novel physical behaviors.

Transformative advances in our understanding of the complex physics at the forefront of materials research, require a deep understanding of the underlying dynamical properties. In hard condensed matter and biology, new materials are often available in limited quantities, particularly as single crystals. Increasing measurement sensitivity to enable studies on smaller samples is therefore considered one of the highest priorities for the design of a new inelastic spectrometer at STS. Lowering the limits for measuring weak scattering will open the door to highly impactful early studies of the most interesting new materials. CHESS is the direct geometry spectrometer that will make such measurements possible. Indeed, the basic design choices for CHESS such as the beam size at the sample position, the targeted energy resolution range (2-5%), and the detector array covering $\Omega \sim 2\pi$ sr all aim to maximize the scattering signal detected for small samples (~mm^3). Monte Carlo simulations will be used to fully optimize the spectrometer and characterize its background to enhance signal-to-noise ratio. This is very important to avoid artefacts in the data set, and for data analysis.

The wide wavelength band employed by this instrument (see Instrument Description) naturally lends itself to performing survey-type experiments and to study materials where dynamic processes exist over a wide energy range. The high flux and the possibility of using Repetition Rate Multiplication (RRM) mode will increase the quality of the data set and decrease the collection time. For this reason, CHESS will often be the instrument of choice for the first spectroscopic investigation of many new materials. Especially in cases where materials are only available in small quantities, CHESS will enable neutron spectroscopy measurements that cannot be performed today. This will place this instrument in a leading position to enable

experiments on new materials with high scientific impact. Furthermore, the possibility to employ XYZ polarization analysis will enrich the level of information acquired during the measurement allowing to disentangle coherent from incoherent signals and magnetic from structural ones, as well as better characterize magnetic correlations emerging from the anisotropic magnetization distribution of spin-orbital systems.

The scientific and technological environment at ORNL, in which CHESS will be embedded, will be relevant for all science areas discussed below. Combining state-of-the-art cold neutron spectroscopy at CHESS with the world-class computing capabilities at the Oak Ridge Leadership Computing Facility (OLCF) and future resources like quantum computers, will be a key to solve complex quantum many-body problems in condensed matter for decades to come. The materials studied with neutron spectroscopy like quantum magnets and soft matter are becoming increasingly complex. The key signatures in the scattering that need to be resolved will be weaker, more diffuse, and hidden by other processes or correlations of less interest that are also present in the materials. It will be increasingly necessary to integrate neutron scattering experiments with advanced computational methods for data analysis and theoretical modeling. On that front, XYZ polarization analysis will also allow to better differentiate between models that would be indistinguishable in absence of spin-space sensitivity. ORNL has the capabilities and personnel to develop a synergistic program, in which theory and experiment go hand in hand, to address the grand challenges of contemporary condensed matter research and to provide world-leading capabilities for US researchers. CHESS has the following distinguishing characteristics from all other ORNL spectrometers:

- Ability to measure small samples (~mm^3) thanks to his high flux.
- Ability to phase the choppers to employ Repetition Rate Multiplication (RRM).
- Ability to efficiently trade flux for energy resolution.
- Ability to employ XYZ polarization analysis.

In the following sections, we present several key research areas that would greatly benefit from the unique capabilities of CHESS.

1.1 QUANTUM AND NANOSCALE MAGNETISM

Quantum fluctuations may prevent the formation of conventional magnetic order in a quantum magnet, and the resulting ground state (GS) is characterized by exotic quasiparticles that can be harnessed for future quantum computing applications. The magnetic excitation spectrum, as explored by inelastic neutron scattering provides fundamental information to understand the nature of these quasiparticles. These excitations contain the fingerprint of the underlying quantum correlations in the system and often exist at low energies, requiring the use of cold neutron spectroscopy. Beyond the canonical spin excitations expected from broken symmetry states, such as phonons and magnons, the excitations of quantum disordered materials often take the form of a continuum of scattering in both energy and wave vector. Understanding the nature and interactions of the fundamental quasiparticles, gauge field excitations or other collective modes that give rise to these continua is a gateway to harnessing the quantum behavior of matter. Consequently, cold neutron spectroscopy investigations of quantum magnets represent an important avenue to identify spin liquids, study the signatures of entanglement, understand coherence and renormalization of quasiparticles, and discern fractionalization from strong quasiparticle interactions. Such quantitative studies are often not feasible with current neutron instrumentation due to the weak, diffuse nature of the continuum signal or the inability to grow large samples with minimal chemical disorder. The greater than 10-fold increase in monochromatic neutron flux on CHESS compared to current best-in-class spectrometers is essential to enable next-generation studies of fractionalization and entanglement in magnetic matter.

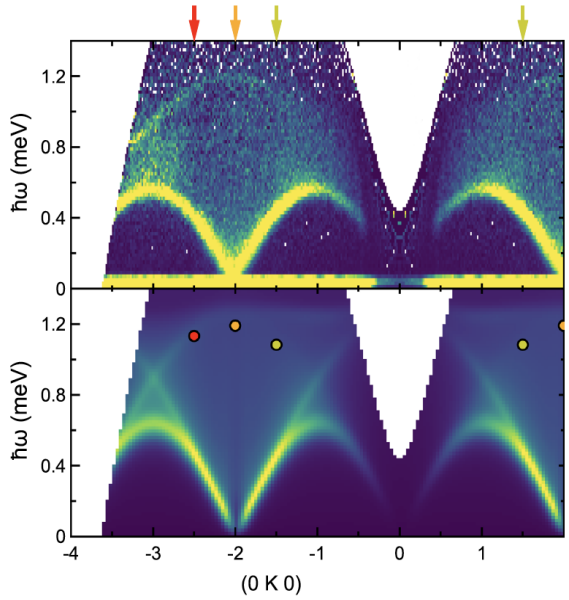

Figure 1-1 ***G. Sala, et al. 2021, "Van Hove singularity in the magnon spectrum of the antiferromagnetic quantum honeycomb lattice".*** *Inelastic neutron scattering data found evidence for a continuum, previously theorized by Van Hove as a singularity in the magnon spectrum. Linear spin wave calculations applied to the Heisenberg model were used to study the physics of this system.*

CHESS will transform our ability to probe excitations in quantum magnets; it will detect weaker and more diffuse signals than existing instruments in its class and offer neutron polarization analysis when it is advantageous. Polarized neutron studies using CHESS will drive a paradigm shift in the ability to probe quantum magnetism. Key experiments will involve probing the spin-space structure of quantum continua as a function of momentum, energy, and external tuning parameters such as temperature. This instrument will provide essential information about the fundamental interactions and processes in quantum materials that give rise to their unique properties, with sufficient energy resolution to measure small gaps, mode splitting, or finite line-shapes in an excitation spectrum. In many cases this is crucial to confirm the ground state of a material and also serve as the fingerprints of collective quantum phenomena as shown in Figure 1.1 [Sala et al. 2021]. In other studies, where temperature will be varied over several tens of K, polarization analysis will enable the study of coherent excitations from the classical regime through the crossover to quantum behavior by minimizing both the coherent and incoherent nuclear background and cleanly revealing the evolution of the spin-structure of excitation continua. By elucidating the spin-space anisotropy of magnetic correlations, polarization analysis will allow better models to be extracted from data and enable more accurate predictions for the existence and stability of quantum phases in magnetic materials.

For example, the quantum spin liquid (QSL) is a well-known state for the ground state in a material that is dominated by quantum fluctuations [Balz et al. 2016, Paddison et al. 2017]. Defining characteristics of such a state are the absence of magnetic order in the zero-temperature limit; a high degree of quantum entanglement; and the presence of continuous, non-local excitations. It is difficult to *directly* confirm these characteristics experimentally and to measure the degree of quantum entanglement. Topological quantum materials offer great potential for dissipation-less electronic transport and topologically protected quasiparticles. This is an area of intense current research activity. The discovery of a skyrmion lattice in MnSi is perhaps the best-known example [Mühlbauer et al. 2009]. Topological spin structures of potential interest are known to exist at zero magnetic field but may also be stabilized in a magnetic field [Martin and Batista 2008, Kamiya and Batista 2014, Leonov and Mostovoy 2015]. One of the challenges here is to distinguish intrinsic multi-**Q** structures, such as skyrmions and vortex crystals, from multiple domains with single-**Q** ordering (each domain has a spiral ordering along a particular direction). By simultaneously probing different energy scales though its repetition-rate multiplication capability, CHESS will unlock the inherent complexity of hierarchical magnetic textures.

In complex functional materials, emergent excitations can arise from hybridization of different degrees of freedom or from finite size effects. The ability to separate nuclear, magnetic and spin-incoherent scattering by polarization analysis will enable measuring the separation of phononic and magnonic or crystal field excitations to a hybridized mode and enable the rejection of spin-incoherent scattering *e.g.,* from hydrogen or cobalt. Polarization analysis at CHESS will enable new discoveries. Examples include: entropy stabilized materials, where magnetic cations present a formidable challenge for understanding the well-defined magnetic excitations that develop in the presence of extreme disorder and their interaction with lattice excitations [Zhang et al. 2019]; the dynamics of magnetic nanoparticles, where the coherent procession of the full particle moment in magnetic nanoparticles is possible, but notoriously difficult to characterize with existing neutron scattering instrumentation [Disch et al. 2015]; or phonon and magnon character in low-energy electromagnons, *e.g.* in delafossite [Seki et al. 2010]. The compact STS moderator and optimized octagonal guide system of CHESS will yield a well-behaved resolution function in a broad range of momentum-energy space, facilitating the modeling of hybridized excitations and their limited lifetime.

For these systems, high-quality single crystals, and the ability to simultaneously reach millikelvin temperatures and high magnetic fields will maximize the unique insights derived from inelastic neutron scattering. Additionally, the need for this capability was explicitly identified in a recent DOE Basic Research Needs workshop: "… neutron scattering instrumentation able to probe all relevant aspects of quantum materials with greater efficiency and a broader range of thermodynamic parameters is needed: Broadband high efficiency inelastic neutron scattering that can provide detailed and comprehensive mapping of spin-resolved electronic correlations in small single crystalline samples (<1 mm^3) from mK to 1000 K … " [DOE 2016]. Available high-quality crystals are frequently small (for example, when they are grown from flux), and their study requires the leap in capability that CHESS will provide, together with a competitive edge for the early characterization of new materials exhibiting low-temperature magnetism. The small and homogenous circular beam spot of CHESS will produce a paradigm shift in sample size requirements.

1.2 MATERIALS TUNED TO CRITICALITY AND BEYOND

The optimization of CHESS for a small beam, ~1 cm^2 at the sample position, will be highly beneficial for studying samples at high pressures or under other extreme conditions that tend to require small sample volumes. Progress in the synthesis of large diamonds via chemical vapor deposition will enable the design of new diamond anvil cells to reach > 10 GPa pressure in a volume large enough for inelastic scattering at CHESS. Pressure is a relevant and clean thermodynamic variable for many materials and physical phenomena, for example, superconductivity and quantum criticality. As an alternative to hydrostatic pressure, chemical doping is also routinely used to introduce chemical pressure in a material. This avoids the restriction on the sample size imposed by high-pressure cells and thus often produces profound results. For example, high-temperature superconductivity is found only when parent copper-oxide insulators are chemically doped [Orenstein and Millis 2000, Lee et al. 2006]. However, chemical substitution necessarily introduces disorder, which may obscure the underlying physics.

Phases like unconventional superconductivity often emerge upon suppression of a competing magnetic phase. In the zero-temperature limit, a material enters a quantum critical regime; and the associated fluctuations are of interest for a range of phenomena in correlated materials. In *f*-electron metals, for example, the interactions are mediated via the conduction electrons that simultaneously screen magnetic 4*f* moments, a process known as the Kondo effect. The competing interactions give rise to an overall low energy scale for spin fluctuations that produce large effective masses for the conduction electrons, leading to an overall low-energy scale for spin fluctuations. Moreover, non-Fermi liquid behavior and unconventional superconductivity typically emerge near the quantum critical point that separates the magnetically ordered state from the heavy fermion phase. In these materials, hydrostatic pressure tends to

be a much cleaner tuning parameter than chemical pressure, and the highest T_C values are found in doped materials or in undoped materials under pressure [Pfleiderer et al. 2009].

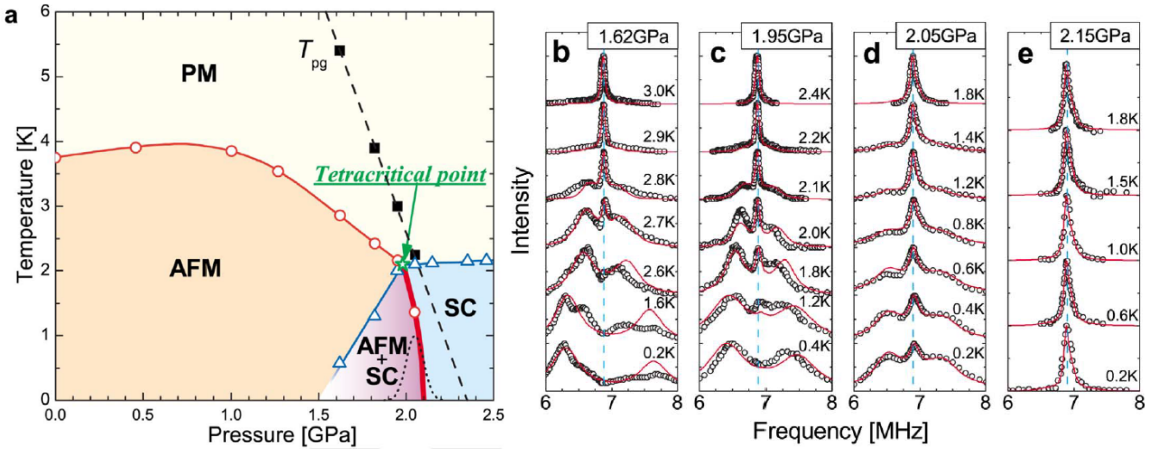

Figure 1-2 ***M. Yashima, et al. 2007, "Quantum phase diagram of anti-ferromagnetism and superconductivity with a tetracritical point in $CeRhIn_5$ in zero magnetic field".*** *(a): The pressure-temperature phase diagram constructed from NQR measurements showing T_N lines (red) for the coexisting AFM phase and AFM+SC phases. (b-e): Temperature dependence of ^{115}In-NQR spectrum at different pressures.*

Quantum critical systems are intrinsically weak scatterers as a result of the small magnetic moments. The increased brightness at STS will enable measurements of these systems that were previously not possible. As quantum critical fluctuations occur over a wide range of energies, repetition rate multiplication at CHESS will offer the flexibility to collect data at all relevant incident energies simultaneously. Previous neutron work on quantum critical points in materials such as $YbAlB_4$ [Okawa et al. 2010], CePdAl [Fritsch et al. 2014], and $CeRhIn_5$ [Yashima et al. 2007] (see Figure 1.2) identified pressure-induced phase transitions. Attempts to probe the spin fluctuations at pressure were largely unsuccessful because of the resolution limits of the instruments and the low signal-to-noise ratio achieved with the available pressure cells. The combination of the various technological advances (higher brightness beams, repetition rate multiplication, larger detector solid angle, 3D-printed collimators, and better pressure cells) will enable significant improvements for such studies at CHESS to reveal the underlying critical scattering.

Ferroelectric quantum criticality is another example that can be strikingly different from its better-known ferromagnetic counterpart [Rowley et al. 2014]. The relevant excitations are soft phonon modes, and the quantum fluctuations are atomic tunneling states. The tunneling frequencies should appear as splitting in the ground and excited state phonon levels, introducing a 'fine' structure in the lattice dynamics that would be well matched to the capabilities of CHESS.

1.3 THERMOELECTRIC MATERIALS

Thermoelectric materials are at the heart of waste-heat recovery devices and find use, for example, in the automotive sector, electrically driven refrigeration, and thermometry. If the conversion efficiency can be further improved, new fields of applications will become viable. For example, replacing classical batteries by thermoelectric generators would be desirable in many places. Such devices have high reliability, no moving parts, and therefore long maintenance intervals, all of which are attractive features.

The thermoelectric figure-of-merit of a material is good when the thermopower is high while the thermal conductivity is low. The latter has two main contributing terms: from band electrons and from phonons (collective lattice vibrations). The thermal conductivity will be low when the free propagation of phonons

is in some way blocked, for example, through scattering by other phonons or lattice defects, or by localization.

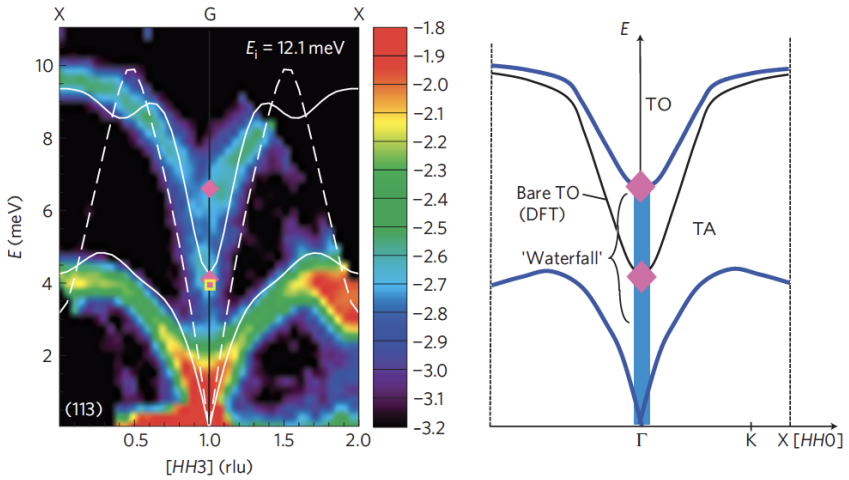

Figure 1-3 ***O. Delaire, et al. 2011, "Giant anharmonic phonon scattering in PbTe".*** *Left: Phonon dispersion measured along [HH0] on the (113) zone, showing the "waterfall" at the Γ-point. Right: Schematic representation of the dispersions (blue lines), with extra diffuse scattering (magenta) and the bare TO branch (black line).*

Inelastic neutron scattering research examining the role of phonons or magnons in the heat transport properties of thermoelectric materials is currently an area of great recent success among the US science community [Delaire et al. 2015, Li et al. 2015, Manley et al 2019, Zheng et al. 2019]. The key factors for this success are the comprehensiveness of the scattering data, $S(\boldsymbol{Q},\omega)$, being measured in four dimensions in combination with first principles calculations. A future possible direction for this research, which would make full use of the enhanced capabilities provided by CHESS, would be to move toward nano-structured materials with larger unit cells, which may feature a broader and more complex spectrum of low-energy modes [Minnich et al. 2009].

1.4 BATTERY MATERIALS

Storage systems for electrical energy are advancing rapidly. Grid stability, especially for intermittent fluctuating nature of renewable energy sources (wind, solar etc.), has huge impacts on modern society including personal computers, smartphones, cars, home security systems, and many other applications. Achieving better performance from a battery in terms of storage capacity, the number of recharging-discharging cycles, and reliability requires a more detailed understanding of the underlying electrochemical processes at the molecular level.

Fundamental research on battery materials to improve their performance is of vital importance. For example, some members of the lithium-orthophosphate family of materials (LiMPO$_4$, M=Mn, Fe) are attractive candidates for electrodes in lithium-based rechargeable batteries because of their high Li-ion conductivity through channels in the olivine crystal structure. These materials are complex and by no means well understood, particularly *operando* when a current is flowing. The ability to predict battery lifetime and capacity, and to design materials with improved properties, is limited. Similarly, understanding oxygen ionic mobility in perovskite and Ruddlesden-Popper type materials is a great challenge for solid-oxide cells. Inelastic neutron scattering is a critical technique to identify the energetics of oxygen diffusive pathways [Paulus et al., 2008]. Obviously, a huge body of work is being done in this area of research; and neutron scattering has a role, as it directly reveals the structure and dynamics of the materials at the atomic level.

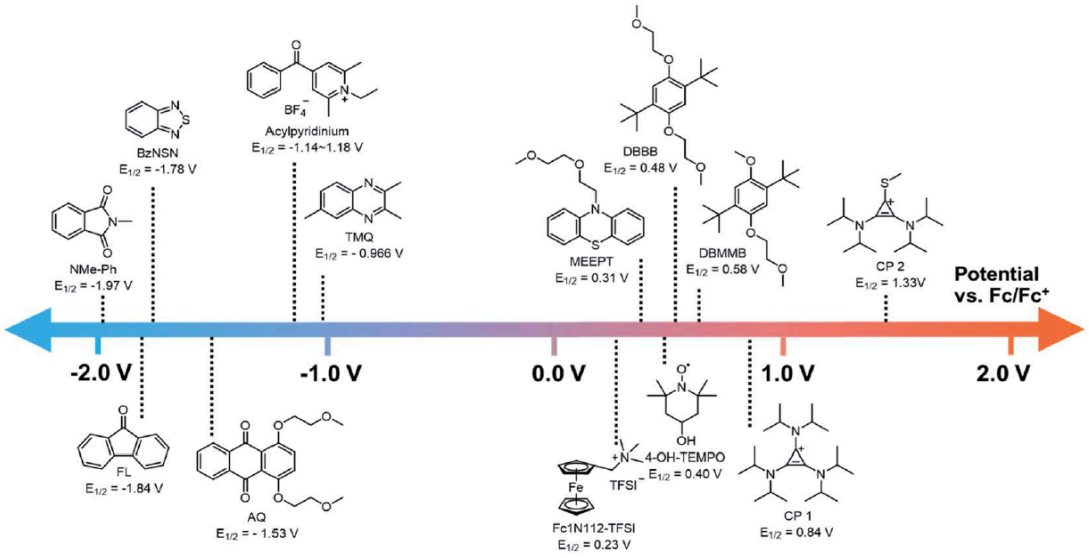

Figure 1-4 ***L. Min, et al. 2020, "Recent advancements in rational design of non-aqueous organic redox flow batteries".*** *Summary of the redox potentials of the state-of-art example ORMs studied in NAqRFBs.*

Another important category where CHESS capabilities will enable new discoveries is electrolyte solutions, such as used in Redox Flow Batteries (RFB) [DOE Energy Innovation Hub]. One advantage of RFB is that energy and power are decoupled, so the technology can be easily scaled up [Rhodes 2020, Wang 2012 and Li Min 2020]. The solvation environment around the working ion in RFB controls nearly everything that happens in the battery, like destructive chemical reactions of the working ion in the electrolyte, the mobility of the working ion as it moves between the anodic and cathodic compartments through the electrolyte, and the reactions of the working ion with the redoxmers that store and release energy causing the battery state of charge (SOC) and discharge [Robertson 2019, Zhixia 2020]. The equilibrium structure of solvation shells at rest depends on the balance of all ion-molecular energetics and entropic drives in the electrolytic solutions. External perturbations, such as electrified interfaces and changing the state of charge in the battery, alter the character of such balance, thus the study of the dynamic response of the liquid solvation to such perturbation is also important. The combination of the length and time scale covered by CHESS (fast motions) with other QENS techniques such as backscattering and NSE (slow motions) is essential to obtain a complete molecular-level understanding of the structure (solvation, aggregation, ion pairing) and dynamics (diffusion, viscosity, conductivity) of electrolyte solutions, especially at high concentrations and at interfaces, even *in situ* [Luo Peng et al. 2020].

1.5 LIQUIDS, COMPLEX FLUIDS AND SOFT MATTER

Neutron scattering is an invaluable tool for studying the structure and dynamics of liquids, complex fluids and soft matter because they are often rich in hydrogen, and the neutron scattering lengths for protons and deuterons are vastly different. It is thus possible, by selective deuteration, to highlight particular parts in a molecule without significantly changing its nature chemically and to tune the contrast in a scattering experiment to preferentially reveal certain aspects of a soft material.

Quasi-elastic and inelastic neutron scattering (QENS/INS) are widely used for measuring mainly the self-motion and sometimes collective dynamics, respectively, in soft materials. Many soft materials exhibit dynamics across a wide energy/time range, often over many decades (from ps to ms and slower). Today, it is often necessary to combine data from two or more instruments operating in different energy windows to gain a complete picture. An instrument like CHESS, which operates in a wide energy window, is thus particularly well suited to studying the dynamics in soft materials, as it can probe a broader, more significant

fraction of these processes simultaneously. The increased cold neutron flux and the high brightness at CHESS will not only enable neutron spectroscopic experiments on samples of small volumes and low concentrations, but also experiments with a high throughput of samples in a series where compositional parameters are being changed. It may also be possible to look at kinetic phenomena, for example, a small volume under shear, to see how these materials respond dynamically to real-life situations. Many soft materials, such as melts of polymers, but also simpler molecules that are liquid at ambient conditions are known to undergo a glass transition on cooling. This is an old but still current topic, and neutron scattering has provided some insights [Doster et al. 1989, Frick and Richter 1995]. Again, the wide energy range in which CHESS simultaneously collects data, and the increased sensitivity to small signals, may provide new impetus for this research area.

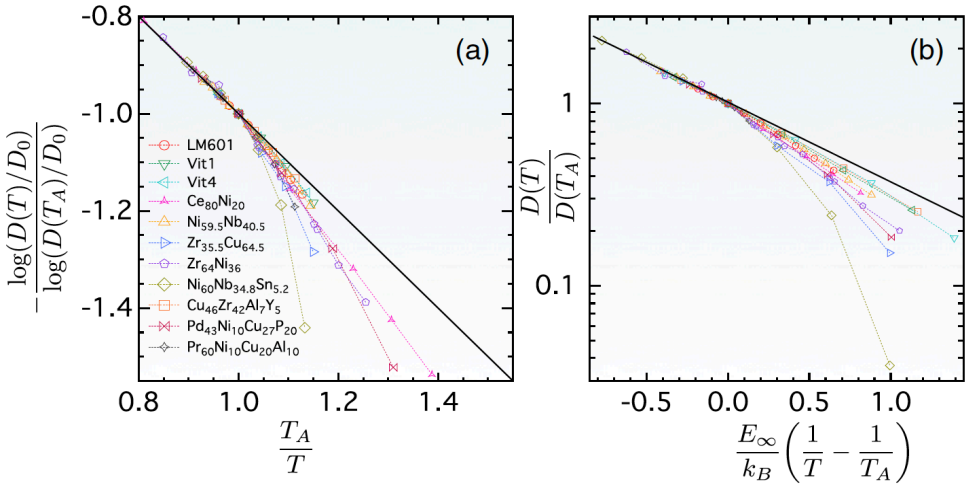

Figure 1-5 ***A. Jaiswal, et al. 2016, "Correlation between fragility and the Arrhenius crossover phenomenon in metallic, molecular, and network liquids".*** *(a-b): Arrhenius crossover in 11 metallic liquids measured using QENS showing the mean diffusion coefficients. Solid lines represent the Arrhenius law.*

Liquids, sometimes falling into the soft matter category, are a distinct class of matter. Indeed, liquids are ubiquitous on earth and prototypical disordered condensed matter systems [Chandler 2017, Walter 2018]. Their very existence is remarkable, thanks to the delicate balance between interparticle potential and entropy. The phase behaviors of liquids and liquid-like matter, especially when driven out of equilibrium by extreme conditions, are exceptionally rich. Accordingly, the physics of liquids have attracted much attention in recent decades. In addition, numerous soft and biological materials of amazing far-from-equilibrium complexity seem to share many intriguing features of liquids. Therefore, quantitative descriptions of the structure and dynamics of liquids and liquid-like matter will likely impact a wide range of disciplines in physics, chemistry, and materials science and engineering. The length and time scale CHESS can cover is perfect to study from slow relaxational or diffusional motions to collective excitations, both propagating and localized modes, in liquids of various interactions, such as molecular, metallic, and ionic liquids [Jaiswal et al. 2016, Ke Yang et al. 2016].

One example is salt or electrolyte solutions. The application of redox active molecule electrolyte solutions highlighted in the previous battery materials section can also fall into this category. In addition, aqueous solutions of salts are the focus of continuing scientific interest because of their relevance in chemistry, biology, and physics. In fact, the presence of ions plays a critical role in many processes, for example in biology, in the selectivity of ion channels; highly concentrated aqueous salt solutions are also the object of increasing interest in the search of novel electrolytes for better performing batteries. Despite intense scrutiny, one of the most intriguing phenomena, the reduction of the viscosity observed for aqueous solutions of certain salts, is still not fully understood. In fact, no significant difference has been observed

in the way the molecular structure of water is affected by the presence of kosmotropes (which increase the viscosity) or chaotropes (which decrease the viscosity) salts in solution. Spectroscopic and computer simulations studies suggest that the effect of salts on the H-bond lifetime is mostly limited to the first solvation shell. CHESS will enable QENS studies of the structural relaxation in aqueous solutions of kosmotrope (structure maker) and chaotrope (structure breaker) salts. Such studies on the kosmotropes and chaotropes influence the solution's viscosity by impacting in opposite ways the hydrogen bond network of water, strengthening it in one case and softening it in the other, and may provide a new perspective to the understanding of the effect of salts on water, underlying the relevance of the hydrogen bond network dynamics beyond a physical picture, strictly structural, and the insight from spectroscopic studies of the H-bond lifetime [Luo Peng et al. 2020].

The additional polarization analysis capability of CHESS will allow us to separate coherent from incoherent scattering from soft materials. In some cases, deuteration will not necessarily be required anymore. Deuterated materials also have a non-negligible incoherent cross-section limiting the effectiveness of the technique. Including polarization analysis on the CHESS instrument will greatly expand the systems we can study with INS. Furthermore, it opens more possibilities to study collective motions in soft and biological materials. In the past, this was most often examined using a Neutron Spin Echo (NSE) instrument, but CHESS will cover a completely different *Q*-*E* space (larger *Q* and higher *E*), than a NSE instrument, thus it will be able to examine localized modes more efficiently.

1.6 HIGH TEMPERATURE LIQUIDS

The wide-angle detector coverage of CHESS, combined with fast data acquisition of small samples, is an ideal fit for container-less processing techniques currently developed at ORNL. The Neutron Electrostatic Levitator (NESL) [Mauro et al. 2016] is frequently used for the study of deeply undercooled molten alloys and is currently one of the only sample environments available in any user program that can support spectroscopic studies of these systems. Studies of liquid dynamics rely on accessing a wide *Q*-range of reciprocal space, to avoid termination ripples in the requisite Fourier transforms, which swamp out the crucial subtle features in disordered systems. Combined with kinetic limitations on resolution, careful determination of the Van Hove function often requires stitching spectra coming from several incident energies. Metastable states, such as deeply undercooled melts, require small samples, rapid cooling and are frequently only stable on the order of seconds, making current spectroscopic experiments exceedingly challenging. CHESS solves all these problems employing its high flux with RRM mode and large detector coverage.

A prominent example shown in Figure 1.6 comes from a series of experiments on electrical transitions in deeply undercooled ($\Delta T \sim 350K$) liquid $Co_{80}Pd_{20}$. Using an electromagnetic levitator with small spherical samples, a clear signal of a second order transition in the specific heat was coupled with anomalies in AC susceptibility, levitation force, and muon spin resonance, consistent with the onset of magnetic ordering [Reske 1995, Wilde 1996, Albrecht 1997]. The lifetime of this state was only a few seconds due to the deep metastability, and no neutron scattering experiment has ever been successfully performed to elucidate the nature of the ordering. While alternate candidate materials are being developed in the NESL program, CHESS will enable probing at the timescales and samples sizes required to obtain the first spectra at multiple incident energies of interest.

Additionally, with careful sample selection and isotopic substitution, QENS enables a microscopic probe of the diffusive behavior of individual species in molten liquids. This information is critical as an input to design new materials suitable from casting to additive manufacturing. Traditional capillary measurements suffer from large uncertainties due to convective effects or chemical reactions; diffusion constants obtained via QENS have significantly smaller uncertainties [Meyer et al. 2008]. Similar measurements at the FTS required timescales of several hours per temperature, eliminating measurement of the undercooled state; obtaining full spectra in seconds would enable access to undercoolings of 300 K or more, relevant to many exotic liquid states.

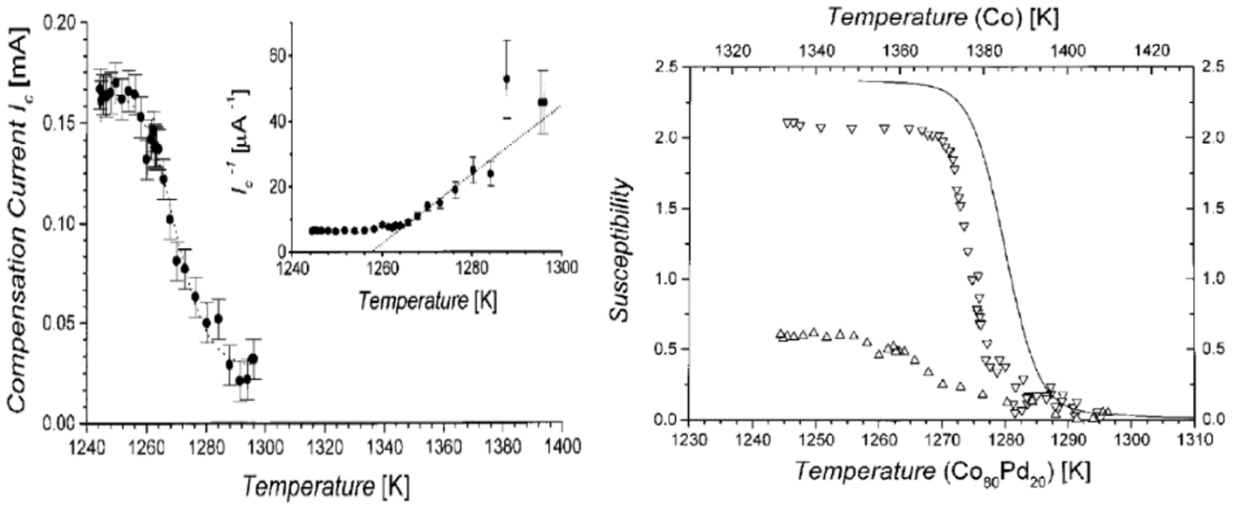

Figure 1-6 ***T. Albrect, et al. 1997, "First observation of ferromagnetism and ferromagnetic domains in a liquid metal".*** *Measurements of the compensation current and the susceptibility vs. temperature of a liquid undercooled $Co_{80}Pd_{20}$ sample, show below 1260 K a plateau of spontaneous magnetization in the liquid metal due to the limited external field of the permanent magnet and its influence on the formation of magnetic domains in $Co_{80}Pd_{20}$.*

1.7 LIFE SCIENCE

The dynamical properties of biomolecules are essential to their function. The past decade has seen enormous progress in the use of neutron scattering in biology. Today, it is possible to study the dynamics of a protein [Nickels et al. 2012] and its hydration water [Perticaroli et al. 2017] in isolation, distinguishing their mutual roles in the dynamics of protein function. Beyond this, neutrons have been used to study the structure of biomembranes [Nickels et al. 2017] as shown in Figure 1.7, and dynamics of proteins [Anunciado et al. 2017] within living cells. However, biological systems are extremely complex; and isolating scattering features from individual components within crowded and diverse biological systems requires extensive bio-deuteration efforts, along with sample mass requirements that are prohibitive for most of the biological community.

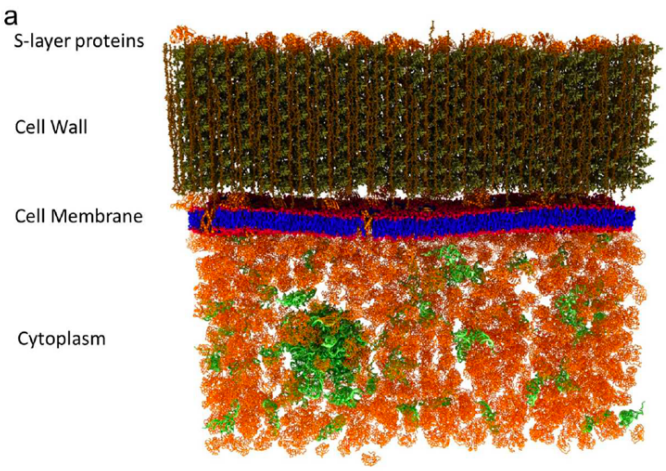

Figure 1-7 ***J. D. Nickels, et al. 2017, "The in vivo structure of biological membranes and evidence for lipid domains".*** *Representation of the cell wall, the membrane and a portion of the cytoplasm of B. subtilis. By tuning the isotropic content of hydrogen within the membrane, and other parts of the bacterium, neutron scattering can be used to study the signal coming from the different parts of the bacteria.*

The new capabilities of CHESS will enable the next generation of scattering experiments in biological systems with increased flux to reduce sample mass requirements and polarized beam capabilities that will allow the separation of coherent and incoherent scattering processes in hydrogenous materials. The latter correspond to collective and single-molecule dynamics, respectively [Gaspar et al. 2010, Burankova et al. 2014]. One example of how coherent neutron scattering might be extended is the demonstrated sensitivity of neutrons to low-frequency vibrations in proteins. The low-frequency vibrations of proteins reflect the global rigidity of the folded protein's secondary structure [Nickels et al. 2013, Perticaroli et al. 2013]. Recently, other forms of vibrational spectroscopy (optical Kerr-effect spectroscopy) have identified changes in protein low-frequency vibrations upon binding to substrates [Turton et al. 2014].

2. INSTRUMENT REQUIREMENTS and DESCRIPTION

2.1 INTRODUCTION

The key capabilities of CHESS that are required by the science case are summarized in Table 2.1. These capabilities are also the main drivers for the physics and technical instrument concepts (see *CHESS Instrument Requirements Document S04040100-SRD10000*).

Table 2.1: Key capability requirements for CHESS.

Parameter	Description
Beam size at sample	Round, Variable: ∅ = 2-20 mm
Detector solid angle coverage	Ω ~2π sr
Incident energy range (ΔE)	$0.2 \leq E_i/\text{meV} \leq 20.4$ ($2 \leq \lambda/\text{Å} \leq 20$) (Possibility to use RRM)
Energy transfer resolution ($\delta E/E$)	2%–5% E_i at the elastic line, flexible
Total Bandwidth ($\Delta\lambda$)	7–8 Å
Q-range (ΔQ)	$0.025 \leq Q/\text{Å}^{-1} \leq 10$
Q-resolution ($\delta Q/Q$)	2% – 5%
Polarization	Polarized beam and XYZ polarization analysis
Beam Divergence at sample	Wavelength Independent: FWHM=2.0°

CHESS is a compact direct geometry spectrometer, the distance between sample and moderator is 31.5 m plus another 2.5 m from sample to detectors. A cascade of 3 disk choppers: a monochromatic (M) high speed f_M = 300 Hz double disk chopper, a pulse-shaping (P) high speed f_P = 300 Hz double disk chopper and a frame-overlap (F) f_F = 15 Hz single disk chopper, located at commensurate distances of 1:2:4 respectively, will efficiently employ the Repetition Rate Multiplication mode (RRM), trading flux for resolution. A customized pulse suppressor (H) f_H = 15 Hz double disk chopper will select how many RRM mini pulses will hit the sample per pulse, avoiding overlaps in the data set. Finally, the wide in-plane and out-of-plane detector coverage Ω~2π sr will maximize the number of neutrons captured. See Figure 2-1 for more details.

The main requirement for studying small samples (~1 mm^3) implies that a medium energy resolution of $\delta E/E$ = 1.8%-5% of the incident energy (E_i), will be used most often to achieve sufficient neutron flux (for cold neutron spectroscopy this can be considered coarse resolution). For some science problems, it will be necessary to improve the energy resolution to $\delta E/E$ = 1% of the incident energy. To achieve this, the overall length of the instrument must be ~30 m to match the contribution of the neutron pulse width of the source with the other terms contributing to the instrumental energy resolution [Ehlers et al. 2018]. Given the STS source frequency, f_S = 15 Hz, a wide bandwidth of $\Delta\lambda$ = 7-8 Å will be available at this instrument length. A longer instrument would reduce the available bandwidth for RRM, and the neutron pulse from the moderator would not fully illuminate the P-chopper (pulse shaping chopper) aperture time window, resulting in an intensity loss with only marginal resolution gain. The length of the instrument has been optimized to take full advantage of the STS tube moderator characteristics. Recent finer optimizations of the dimensions of the moderator resulted in a neutron pulse width of about $v\Delta t$~0.23 m, where v is the velocity of the produced neutrons. We employed a new fully automated Monte Carlo fitting procedure to optimize the octagonal elliptic profile of our guide system based on these new tube moderator parameters.

Currently, simulations predict an efficiency in the transport of a white neutron beam ($2 \leq \lambda/\text{Å} \leq 20$) around 70%, while restricting both horizontal and vertical beam divergence to FWHM=2.0°. Furthermore, the final 250 mm of our guide system can be interchanged based on the sample environment and the nature of the experiment to further improve Flux on small samples. More information about the CHESS optics system and related optimizations can be found in the *CHESS Optics Design Description document S04040200-DES10000.*

To maximize the efficiency of a measurement, CHESS can operate in Repetition Rate Multiplication (RRM) mode with 1-8 energies arriving as a sequence of mini pulses at the sample within a single frame (1/15 Hz = 66.667 ms). A flexible scheme to adjust the time window in which energy loss(gain) is observed for each incident neutron energy, has been studied to optimize the design of the H-chopper. Since the amount of time needed to measure a particular energy loss or gain depends on the incident energy, our criteria for standard measurements were to allow only mini pulses that always grant the possibility to measure within $-2.1E_i \leq \Delta E \leq 0.9E_i$ in energy transfer. However, at very high wavelengths, observing quasi-elastic scattering (QENS) that requires measuring only up to ~50% energy loss would allow many more mini pulses to be used than when measuring at higher incident energies. The suppression scheme of the H-chopper is flexible enough to allow such measurements as exemplified in Figures 2-8,2-9, and further improvements including studies of the pulse contamination will be performed during preliminary design.

The scientific design that exploits high solid-angle detector coverage by using high out-of-plane scattering angles and full in-plane angular coverage places a premium on symmetric horizontal and vertical beam angular divergence (see Figure 2-3). The guide system must be straight for optimized neutron transport achieving symmetric beam profiles. Bending the beam out of the line-of-sight over a short distance (~30 m to the sample) would result in too much asymmetry between the right and left sides of the instrument. Therefore, a horizontal T_0-chopper will be needed to block the flash pulse of high-energy particles (neutrons and photons) from the target [Bewley and Taylor 2011]. The P-chopper and the M-chopper can operate in a double-blind configuration mode [Vickery and Deen 2014]. This will ensure that the time width of each neutron mini pulse on the sample will increase with wavelength and will help to make the energy resolution more evenly distributed between pulses when necessary. However, CHESS can also operate in a more traditional way where each mini pulse will achieve better and better resolution, depending on the nature of the measurement. It is also important that CHESS offers polarization analysis from day one of operation, as required by the science opportunities envisioned for this instrument.

Finally, CHESS must be located in the STS 50 m instrument building, which places the instrument as far away as achievable from possible backgrounds generated by the first target station (FTS). Indeed, since inelastic scattering is much weaker than elastic scattering, the ambient background between pulses needs to be as low as possible. Notice that FTS will operate at a higher repetition rate than STS, thus receiving pulses between those directed to STS during the time that CHESS is measuring weak inelastic signals. It is also important to maximize the distance to the possible extreme magnetic field instruments because high magnetic fields will interfere with the operation of polarized ^{3}He cells proposed for neutron polarization analysis at CHESS. Therefore, careful considerations in the placement of these instruments must be considered. Detailed Monte Carlo simulations will be performed to study and identify solutions to minimize any source of background noise, enhancing the signal-to-noise ratio of the measurement.

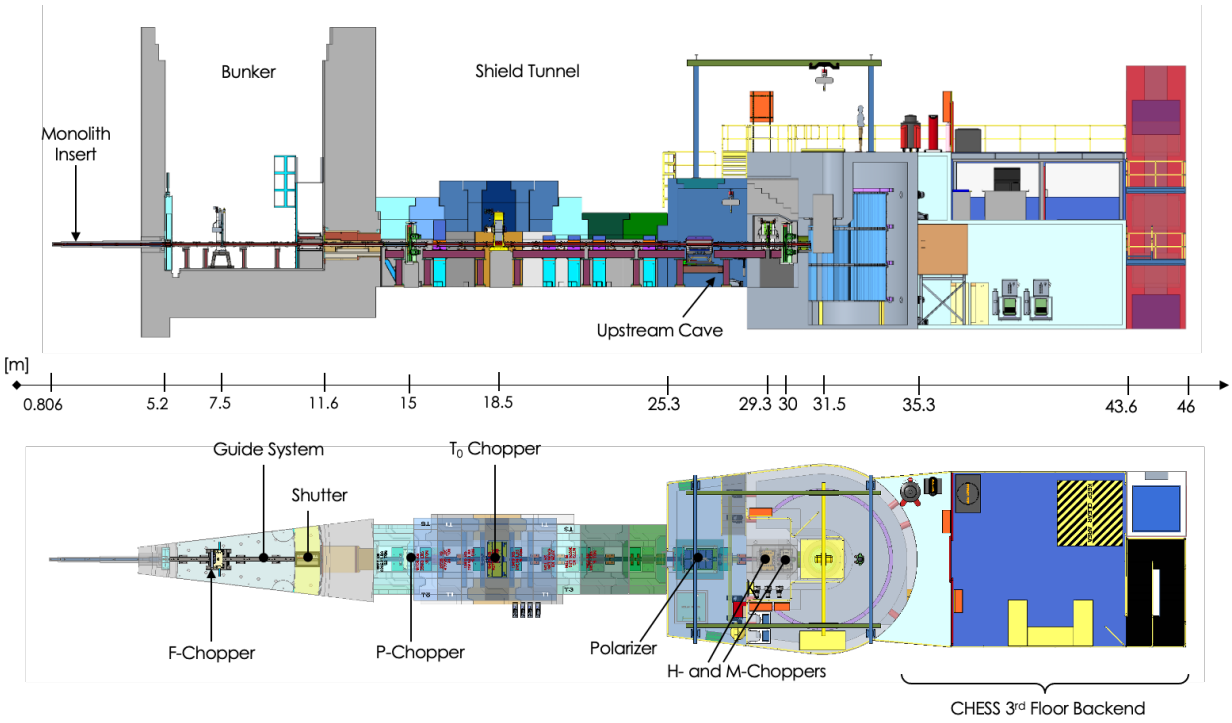

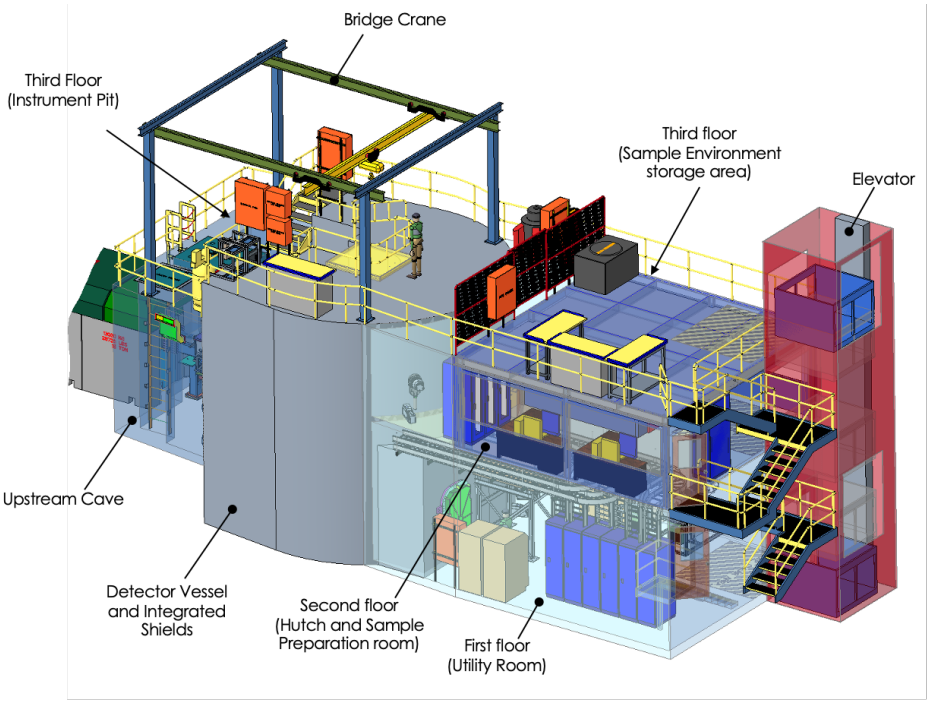

Figure 2-1 Top: The main components of the CHESS spectrometers (see Table 2.1) and their locations along the beamline. The total distance between the ST14 tube moderator and the sample is exactly 31.5 m. Bottom: Overview of the backend of the spectrometer showing the different areas for the detector vacuum vessel (gray cylinder), utility room, hutch, and sample preparation area. The upper level is designed to host an area for sample environment storage and maintenance directly.

2.1.1 CHESS Key Components and Functions

The following Table 2.2 presents a list of the key components of the CHESS spectrometer shown in Figure 2-1 and reported in the *CHESS Instrument Schematic S04040100-CMT10000* and in the *CHESS Optics Design Description document S04040200-DES10000.*

Table 2.2: Key components of the CHESS beamline.

Component	Description	Location from Moderator
	Beam delivery	
Neutron guides	Straight, elliptic octagonal guide with pinch points at the P and M-choppers. Neutron transport.	Z = 0.806 – 31.25 m
F-chopper	1 disk @f=15 Hz, frame-overlap	Z = 7.5 m (in bunker)
Shutter	Shutter for daily operations	Z = 10.5 m
P-chopper	2 disks @f=300 Hz, pulse-shaping	Z = 15 m
T_0-chopper	1 rotor @f=15 Hz	Z = 18.5 m
Transmission polarizer	Polarize the beam, located on translation table	Z = 26.06 m
RF spin flipper	Flip the spin state	Z = 27.11 m
H-chopper	2 disks @f=15 Hz	Z = 29.3 m
Beamline shielding	Radiation Protection	Z = 13.7 m – 25.3 m
M-chopper	2 disks @f=300 Hz, monochromator	Z = 30 m
Aperture system	Tailors beam size and divergence	Z = 31 – 31.25 m
Sample location	Sample	Z = 31.5 m
	End Station	
Shield upstream cave	Radiation Protection	Z = 25.3 – 35.3 m
Detector array	8-packs of linear LPSD ^{3}He tubes	Z = 34 m; R = 2.5 m
Beam-stop	Stop direct neutron beam	Z = 36 m

2.1.2 Instrument Specific Considerations

Based on the science case, the CHESS instrument is required to use high-field-non-compensated magnets, whose stray fields can potentially interfere with the normal operations of the high-speed choppers, and with our polarization devices. Currently, we are investigating solutions to shield the high-speed M-chopper and the H-chopper from the stray fields, mitigating this problem and allowing flawless operations. The theoretical limit of the stray field at the location of these choppers should stay below 60 Gauss. Calculations are on-going to map the field as a function of position to optimize shielding.

Polarization is very unlikely to be used with non-compensated high field magnets, due to the natural incompatibility of the ^{3}He analyzer with high stray fields. During the preliminary phase of the project, we will evaluate possible solutions to shield our analyzer and, eventually, we will set a maximum field for compensated magnets that could be compatible with our polarization system. In the worst-case scenario, where experiments could not be performed at CHESS coupling an external field with polarization analysis, the planned triple axis instrument instrument MANTA at HFIR will supply this capability to the user community.

2.2 GUIDE OPTIMIZATION (WBS S.04.04.02)

Given the small circular tube moderator and sample size, the CHESS guide system has been designed to account for optimization in Flux and Brilliance Transfer (BT) with a uniform divergence profile constrained

within FWHM = 2.0°, which are the two primary figures of merit (FOM) considered in the optimization process. Simulations showed that optimizations for pure flux while disregarding the divergence profiles of the neutrons resulted in a high background mainly due to high divergent neutrons propagating through the guide system, often completely missing the sample. Therefore, the guide system was optimized considering both flux and divergence simultaneously to achieve a perfect balance between these two quantities.

We employed a new procedure for the optimization process which leverages on the combination of McStas [Willendrup 2014], Jupyter notebooks [Hafner 2020] and the SciPy library [Newville 2014]. The McStas CHESS instrument (see App. B) is built using Python functions which offer a natural and easy environment to manipulate the guide profiles. As a starting point, the guide system is composed of three ellipsoidal guides pinched at the P, M-choppers and at the sample position. Our software generates one-dimensional guide profiles as a function of six parameters allowing engineering constraints (*e.g.*, maximum optic dimensions in the monolith are 5x5 cm, and 7x7 cm at the bunker), that are then rotated *n*-times to obtain different cross sections. These profiles are combinations of different half-ellipses joined at their mid-points as sketched in Figure 2-2.

Given the circular shape of the tube moderator, we needed to consider two main problems: 1) guide illumination and 2) how to calculate the volume of the phase space in a non-orthogonal space. For optimal illumination we decided to adopt octagonal cross sections that better approximate the circular shape of the moderator, with a negligible loss in flux. The volume of the phase space was calculated assuming a homogenous and constant divergence profile measured on a 1 x 1 cm^2 area at the sample location.

Once the profile has been generated, our code fitted the parameters of the guide profiles to maximize Flux and neutron transport efficiency for our cost function. This is an iterative procedure that is handled directly by the SciPy library, and we used different methods (*e.g.*, SLSQP, Powell, Nelder-Mead, BFGS) to explore the parameter space during our optimization. Finally, once the best set of parameters was achieved, the simulations were repeated to include the correct guide length, gaps for Al windows and choppers housing to optimize the *m*-values and test CHESS performances (see Figure 2-2). Figure 2-3 compares the acceptance diagrams for the current best octagonal and square set of guides. Simulations show that the octagonal guide cross section completely fills the phase space, confirming our initial predictions.

More information related to the optimization of the CHESS optics system can be found in the *CHESS Optics Design Description S04040200-DES10000.*

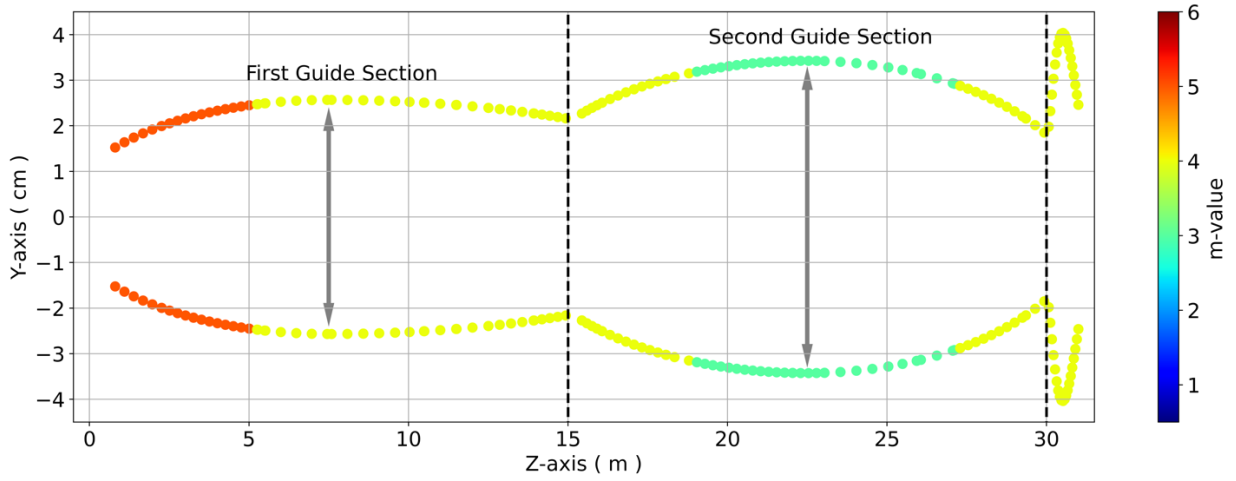

Figure 2-2 Layout of the CHESS guide system showing the refined profiles of the three elliptical guide sections. The profile of the guides is color coded as a function of the optimized m-values of the supermirror.

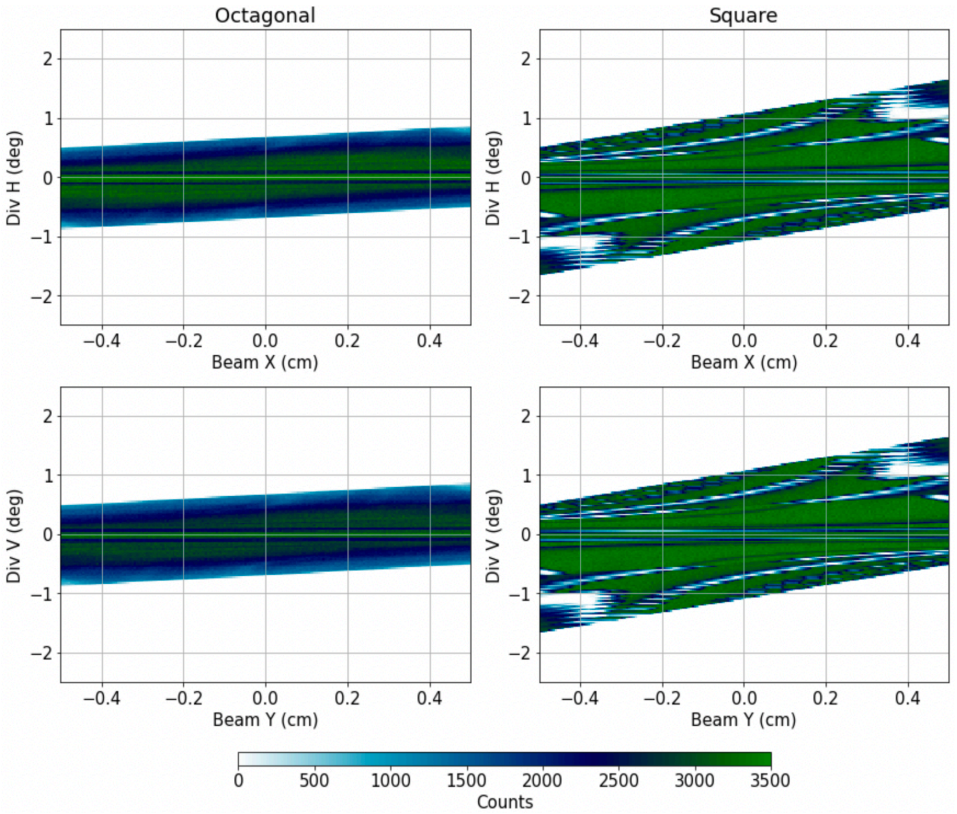

Figure 2-3 Transported Phase-Space simulated at the sample position, for the final optimized set of octagonal (left) and square (right) cross-section elliptical guide system.

2.2.1 Octagonal Guide Performances

The octagonal cross section has been originally selected to solve the problem of illumination due to the circular shape of the tube moderator. A traditional square guide cross section could suffer from over(under)-illumination, resulting in loss of flux or gaps in the transported phase space. Other guide cross sections like hexagonal, decagonal, dodecagonal have been analyzed during the optimization phase, but were disregarded due to lower performances or high cost of manufacturing.
Assuming a target sample of 1 cm^2 area, the octagonal profiles offer an excellent compromise between maximizing the neutron transport and minimizing beam divergence (see Figure 2-4), and they can also be manufactured by SwissNeutronics, SD-H and Mirrortron. Our simulations showed that we can obtain a wavelength independent divergence profile, which is very important for RRM mode since it makes the resolution function profile of each energy very homogenous. The guide also maintains an average neutron transport efficiency, calculated as the ratio of the number of neutrons arriving at the sample divided by the number of neutrons entering the first guide, above 70%.

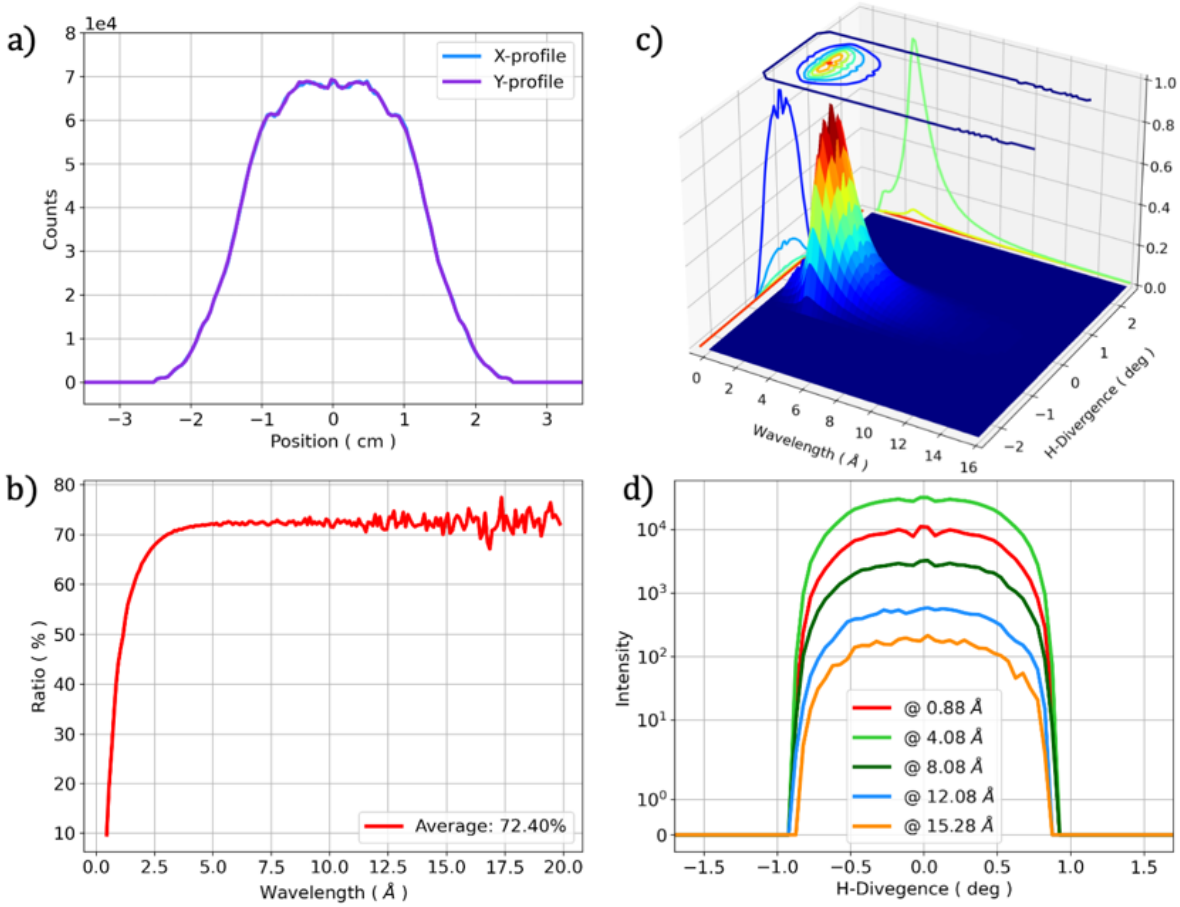

Figure 2-4 a) Beam profile at sample position in horizontal ("X-profile") and vertical ("Y-profile") direction, b) Neutron Transport Efficiency and c-d) Wavelength Independent-Divergence profiles at sample, simulated for an octagonal cross-section elliptic guide system.

2.2.2 Square Guide Performances

The more traditional square guide cross section has also been optimized for the CHESS guide system. The guide entrance was over-illuminated to avoid gaps in the phase space. Assuming a target sample of 1 cm^2 area, Flux and neutron transport efficiency are not drastically different from the octagonal profile shown above. As can be seen in Figure 2-5 both are higher than 70%. However, the divergence profile provided by the square cross section is wavelength dependent, and the phase space is still not perfectly. We were not able to mitigate this situation despite our numerous efforts, thus the option of a square guide cross-section was disregarded.

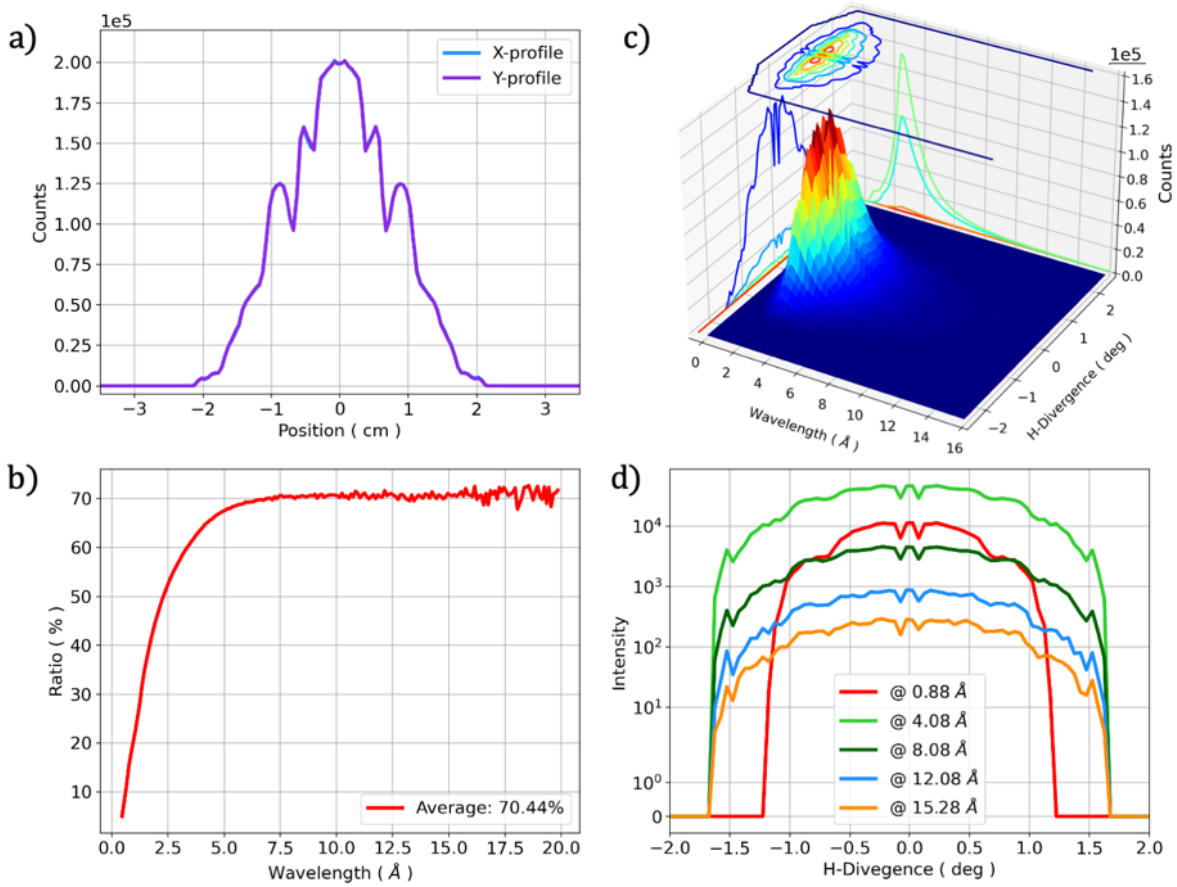

Figure 2-5 a) Beam profile at sample position in horizontal ("X-profile") and vertical ("Y-profile") direction, b) Neutron Transport Efficiency and c-d) Wavelength Dependent-Divergence profiles at the sample, simulated for a square cross-section elliptic guide system.

2.3 CHOPPER DESCRIPTION (WBS S.04.04.03)

The CHESS instrument is equipped with a cascade of 3 double disk and one large single disk choppers for beam manipulation, and one horizontal T-zero (T_0) chopper for high energy neutrons and gamma suppression. Among the 3 double disk choppers the Pulse shaping (P) and the Monochromatic (M) choppers are a pair of counter-rotating high-speed disk choppers ($f \geq 300$ Hz) in carbon-fiber, tailoring the beam to provide a versatile Flux and Energy Resolution at the elastic line. The other two choppers (F) and (H) work as frame-overlap and pulse suppressors respectively. Specifically, the Frame overlap (F) chopper operates at 15 Hz, and it is responsible to select the wavelength bandwidth, while the Hand (H) chopper has a set of different apertures optimized to provide flexible RRM energies (from 1 to 8 mini-pulses) based on the experiment being performed. The possibility to run this chopper at frequencies higher than 15 Hz is currently being evaluated.
Table 2.3 shows a summary of the chopper characteristics. Section 5 of the *CHESS Instrument Requirements Document S04040100-SRD10000*, contains all chopper requirements for the CHESS chopper system.

Table 2.3: Chopper requirements for CHESS.

Chopper Name	Location	Type	Disk Size	Apertures/Disk	Frequency
Frame overlap (F)	7.5 m	Single-Disk	∅ = 1.24 m	1	15 Hz
Pulse shaping (P)	15.0 m	Double-Disk	∅ = 0.7 m	2	≥ 300 Hz
T-zero (T_0)	18.5 m	Horizontal	∅ = 1.24 m	N/A	15 Hz
Hand (H)	29.3 m	Double-Disk	∅ = 0.7 m	$1 \leq \# \leq 8$	15-60 Hz
Monochromatic (M)	30 m	Double-Disk	∅ = 0.7 m	1	≥ 300 Hz

2.3.1 T-zero Chopper Analysis

To effectively employ the Repetition Rate Multiplication Technique (RRM) mode, made possible by the low frequency (15 Hz) of the STS source, CHESS must be a short beamline. However, this characteristic may also be a source of background due to high energy neutrons that will reach the sample though the guide system. Since a bender solution to get out of the line of sight cannot be employed due to space confinement, CHESS will adopt a horizontal T-zero (T_0) chopper located at ~18.5 m. This device will be fully closed for wavelengths below 0.7 Å, and fully opened for wavelength above 1.0 Å to allow the proper wavelength bandwidth to pass. The possibility to use a vertical T-zero chopper was excluded since this device is closed for 70% of the time, thus incompatible with the RRM mode.
In preliminary design we will carefully revise the location of this chopper as well as the shape of the Inconel absorbing wedge employing Monte Carlo simulations, within the framework of background suppression analysis.
Our current chopper engineer Bill M^{c}Hargue provided us with an analytical calculation about the performances of the T-zero chopper for two cases: one where the rotor diameter matches the current 1.24m diameter for the STS choppers, and a second one where the rotor was decreased down to the size of a standard FTS T-zero chopper.

In both cases the chopper spins at 15 Hz. However, to block the appropriate neutron wavelength bandwidth required by the science case, the chopper with the smaller disk diameter will have to be relocated to 45 meters downstream of the tube moderator, which is an unpractical location since the instrument length is much shorter than that. Details of the calculation are provided in Figs. 2-6,2-7.

Parameters

6/19/2023 16:12

Window/Beam size-width	7	cm		
Window/Beam size-height	7	cm		
Chopper Rotor Diameter	124	cm		
Chopper Speed	15	Hz		
Time for edge to clear window	1.35E-03	s		T0 Rotation
Fully Blocked Wavelength	0.7	Å	166.9 meV	17.06 °
Fully Open Wavlength	1	Å	81.8 meV	24.37 °
Velocity of 1 Å neutrons	3956	m/s		

Calculations

Time for edge to clear window	1.35E-03	1.35E-03	1.35E-03
Fully Open Wavlength - Fully Blocked Wavelength	1.0000 - 0.7000	0.3	7.58342E-05
Velocity of 1 Å neutrons	3956	3956	
			17.848 meters
Time for 1 Å neutrons to travel 17.848 meters		=	4.51E-03 seconds

Figure 2-6 T-zero calculation for a 1.24m diameter rotor (current STS style). The chopper must be placed at least 17.85m downstream of the moderator to block the correct bandwidth and to be completely out of the path of the required neutron wavelength by CHESS.

Parameters

6/19/2023 16:14

Window/Beam size-width	7	cm		
Window/Beam size-height	7	cm		
Chopper Rotor Diameter	57.37	cm		
Chopper Speed	15	Hz		
Time for edge to clear window	3.43E-03	s		T0 Rotation
Fully Blocked Wavelength	0.7	Å	166.9 meV	43.18 °
Fully Open Wavlength	1	Å	81.8 meV	61.69 °
Velocity of 1 Å neutrons	3956	m/s		

Calculations

Time for edge to clear window	3.43E-03	3.43E-03	3.43E-03
Fully Open Wavlength - Fully Blocked Wavelength	1.0000 - 0.7000	0.3	7.58342E-05
Velocity of 1 Å neutrons	3956	3956	
			45.189 meters
Time for 1 Å neutrons to travel 45.189 meters		=	1.14E-02 seconds

Figure 2-7 T-zero calculation for a 57.37cm diameter rotor (current FTS style). The chopper must be placed at least 45.2m downstream of the moderator to block the correct bandwidth and to be completely out of the path of the required neutron wavelength by CHESS.

2.3.2 Repetition Rate Multiplication (RRM) H-Chopper Analysis

The CHESS instrument will employ the Repetition Rate Multiplication (RRM) mode, already running at instruments like LET at ISIS and AMATERAS at J-PARC. This mode of operation leverages the low frequency, f_S = 15 Hz, of STS, allowing more than one energy to hit the sample in one neutron pulse. Our analysis indicated that in the best-case scenario CHESS will employ a maximum of 8 incident energies (E_i) per pulse, clearly separated to avoid overlap in the final data set and granting a coverage of $-2.1E_i \leq \Delta E \leq 0.9E_i$ in energy transfer every time. For this reason, the H-Chopper is a double disk chopper with "dynamic apertures" that can change the number of slots from one (classical monochromatic beam) to a maximum of 8, depending on the nominal wavelength.

This chopper must be placed upstream within 0.7 m of the M-chopper, otherwise there will be further energies leaking through the two choppers, defeating the intended purpose. Furthermore, its design has been studied for frequencies between $15 \leq f \leq 60$ Hz to account for different resolutions and flux.

The space between the slots is not only designed to achieve 8 independent energies (see Figure 2-9), covering a bandwidth of $\Delta\lambda$=7-8 Å at nominal short wavelengths (1-1.5 Å), but it also considers super-resolution techniques by allowing only sub-sequent mini pulses with an average ratio of ~$0.57E_i$ of the previous one. This also facilitates obtaining sub-sequent resolutions twice as good. The possibility to employ a similar "dynamic" chopper scheme as the VOR instrument [Vickery and Deen 2014] has also been considered and discarded due to the technical complications associated with the engineering design. Furthermore, this technique does not match the intrinsic STS moderator pulse width, especially at lower energies. Figure 2-8 shows the current proposed scheme for the H-chopper, further analysis on the location of the apertures and related performance are currently ongoing. The final shape of the H-chopper disks will be defined during the final design phase of the project.

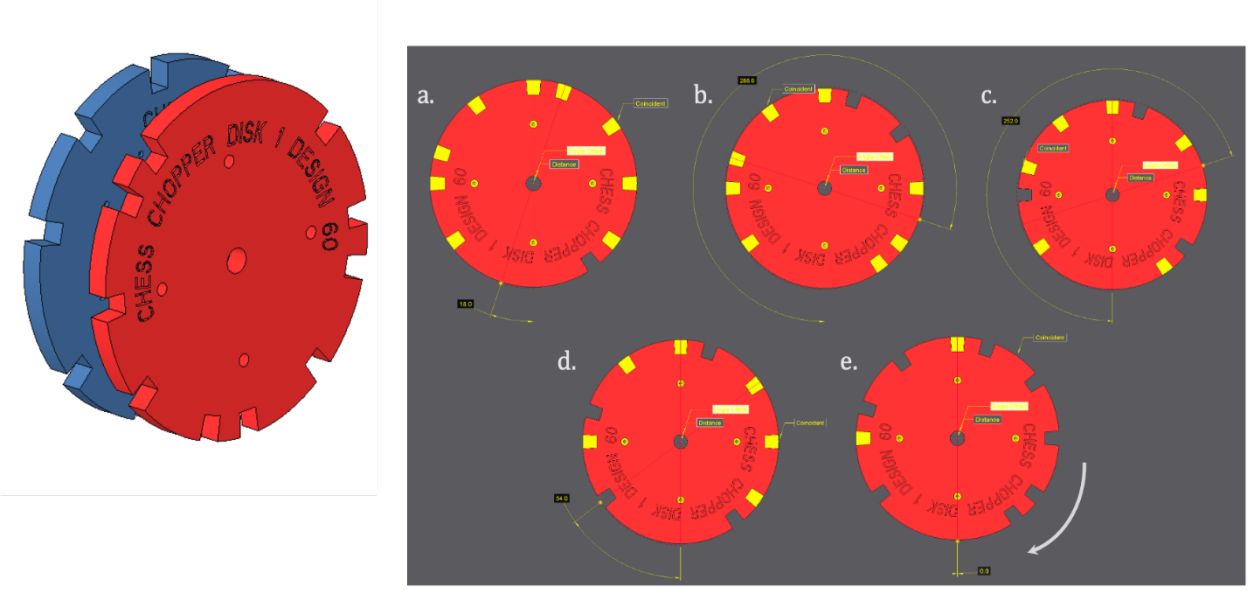

Figure 2-8 Left: Schematic view of the two custom disks of the H-Chopper, designed to employ the RRM mode. Right: By changing the angular phase of the second disks, users can get a different number of apertures i.e., a different number of incident energies. Shown from (a. - e.) are 5 of the 20 possible configurations.

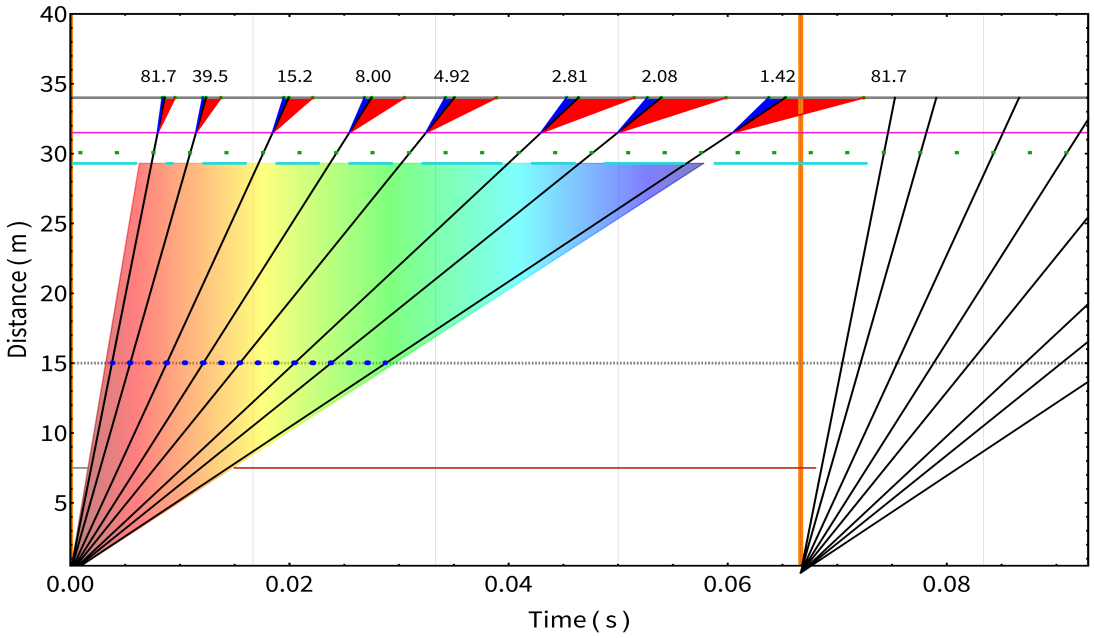

Figure 2-9 Space-Time diagram showing different distribution of several RRMs energies, as a function of the nominal wavelength. The analysis of the H-Chopper disk apertures for 8 apertures shows that each consecutive energy is about $0.57E_i$ of the previous one, with an average FWHM resolution twice as better.

2.4 SHIELDING (WBS S.04.04.04)

The CHESS beamline will adopt the standard shield blocks designed for STS beamlines to maintain the radiation level ≤ 0.25 mrem/h. Customized shield blocks will be used only where needed along the beamline. By utilizing standard shield blocks, CHESS will decrease shield block design time and reduce vendor related costs.

The standard shield blocks will be precast stacked concrete. Both high density and regular density blocks are included in the standardization design. Future neutronics evaluation will determine material selection for shielding blocks to ensure radiation requirements are met. Provisions will be included in the design of the shield blocks to allow for installation and removal. In addition, the shielding blocks will be designed to meet seismic requirements.
Specifically:

- Guides and Choppers will be encased under standard and custom shield blocks which will maintain external area of the transport shield tunnel under 0.25mrem/h
- The vacuum vessel houses the detector system and will be constructed using stainless steel webbing supported by structural ribbing. To meet radiation requirements the cavities of the vacuum vessel will be filled with polyethylene. For background shielding the inner vacuum vessel will be covered with ZHIP tiles. Additional shielding may be provided on the roof to protect against cosmic radiation.
- Neutronics calculations will determine if CHESS requires a movable shield at the top of the sample pit to contain the radiation in that area during operations.
- The backend of the instrument will include provisions to ensure the auxiliary equipment for the vacuum system, detector system, and sample preparation areas have proper radiation protection.

Neutronics analysis will define the thickness of the shields in all the area.

2.4.1 Background Shielding

The CHESS instrument will adopt all the best practices and recent developments in neutron background suppression [Kikuchi 2019] to achieve a low background, high signal-to-noise ratio to satisfy the science case. We already identified some critical area along the instrument that will be investigated in detail with Monte Carlo simulations these are:

- Bunker: Possibility of guide cross-talking, neutrons leaking from and into choppers and high energy neutrons generated from the moderator will be investigated.
- Guide: A set of baffles will be placed along the guide system to stop high energy neutrons from propagating through the guide system. Thickness and texture of the Al and Chopper windows will be minimized to decrease diffuse scattering and flux loss.
- Detector Tank: Monte Carlo simulations will be performed to analyze the crosstalk between He-tubes and opposite detectors facing at 180°.
- Sample Environment: Monte Carlo simulations will be performed to study multiple scattering events between the sample and the sample environment to optimize the geometry of radial collimators.
- Magnetic Fields: A detailed analysis on the stray field generated by sample environment will be performed by our engineers. Based on these results we will make provisions to shield our H- and M-choppers against the stray field, to protect the magnetic bearings. Other components sensitive to remnant magnetization like: rebars, detector frame, detector vessel and He-detectors will also be evaluated. Our estimates suggest keeping a magnetic stray field level below 10 Gauss.
- External Sources: Calculations will be made to estimate the background levels due to future instruments located nearby CHESS.

2.5 DETECTOR LAYOUT (WBS S.04.04.05)

The CHESS instrument will have an unprecedented detector coverage close to $\Omega=2\pi$ sr. The detectors will be Linear Position Sensitive Detector (LPSD) ^{3}He tubes arranged in the standard ORNL 8-pack configuration. Given the possible engineering challenges to assemble and maintain this structure without appreciable deviations of the pixel locations, CHESS will adopt a cylindrical detector geometry as shown in Figure 2-10. 8-pack detectors will be arranged on three arcs; a middle one that will cover an in-plane 2θ angle between ±140° and an out-of-plane angle $-15.6° < \phi < 15.6°$, and an upper and lower arc that will extend the out-of-plane coverage up to ϕ ±40°.
Table 2.4 summarizes the requirements of the CHESS detector array. More details can be found in the document *STS detector needs for STS instruments S04000000-TRT10000*.

Table 2.4: Detector requirements for CHESS.

Parameter	Description
Tube Length	1.4 m
Tube Diameter	∅ = 2.54 cm
Tube Material	Stainless Steel 0.5 mm
Pixel per tube	128 (1024 per 8-pack)
Detector Type	^{3}He Linear Position Sensitive Detector (LPSD)
Detector Arrangement	Standard 8-pack in-line
^{3}He pressure	8 atm

A total of 159 ^{3}He standard 8-pack detectors are required to complete the cylindrical geometry of the CHESS detector array. Each of the three rows hosts 53 standard 8-packs, with tube dimensions as shown in Table 2.4. This configuration restricts the total out-of-plane coverage to $\phi \pm 40°$, but leaves no gaps in the final data set. Analysis on the resolution ellipsoid for this detector geometry and possible relations to symmetry operation artifacts in the data set are currently ongoing.
As in the earlier versions of the 8-pack design, the front-end electronics, and Read-out Controllers (ROCs) of each 8-pack will be mounted directly on the rear of the 8-pack structure. Digitized data will be fed through to racks outside of the vacuum chamber where it will be aggregated into full detector datasets.

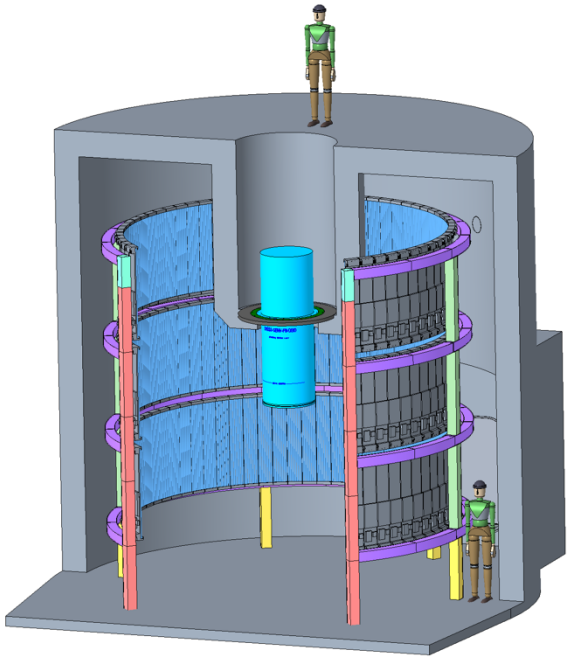

Figure 2-10 CHESS Cylindrical detector configuration housing 159 ^{3}He 8-pack detectors on three rows. The detectors and frame are sitting in a vacuum tank.

2.5.1 Beam Monitors

CHESS will adopt a set of 4 beam monitors, two fixed and two retractable, to monitor the performances of the choppers, the beam profile, guide misalignments and to calculate the emission time of the neutrons. Data will be collected to assess the overall status of the instrument. Currently, we are evaluating the possibility to adopt the ISIS fiber optics, the ISIS beads monitors, as well as the ILL Multi-Tube monitors for both the fixed monitors before and after the sample position and for the retractable monitors located right in front of the F and P-choppers. Each monitor will provide event-based readout allowing for ToF profile reconstruction, while the fixed monitors used for normalization will record total counts over the spatial cross-section of the beam.
More details can be found in the document *STS detector needs for STS instruments S04000000-TRT10000*.

2.6 MONTE CARLO SIMULATION RESULTS

The CHESS instrument performance has been simulated using the software MCViNE [Lin 2016]. Simulations of energy resolution at the elastic line, neutron flux at the sample position in monochromatic mode (see Figure 2-11) and two virtual experiments in Repetition Rate Multiplication (RRM) mode (see Figure 2-12) have been performed to benchmark the accuracy of our predictions reported in Table 2.1.

Overall, CHESS has an energy resolution in excellent agreement with the Ikeda-Carpenter resolution function for the elastic line [Carpenter 1978], which confirms analytic predictions about the locations of the fast speed choppers. Furthermore, CHESS' resolution is in remarkable agreement with CNCS in its high flux mode of operation. These simulations were performed adopting an opening angle of 6 degrees for the Monochromating M-chopper. Comparisons with real data collected at the respective instruments also show that the LET and the AMATERAS spectrometers have higher resolution. This can be achieved by decreasing the opening angle of CHESS' M-chopper down to 3 degrees (high resolution mode). These two opening settings will affect the flux of the instrument as shown in Figure 2-11. In normal high flux operation mode (HF), the comparison using a monochromatic beam (no RRM used) shows that CHESS has currently 30X times more flux than CNCS with a peak of 3e7 n/s/cm^2 at 3 Å, in good agreement with our preliminary expectations. Further optimization on the profile of the third guide may grant an even higher gain to CHESS, but these results are still under evaluation, and they need to be coupled with the analysis of sample environment size and requirements.

The second configuration, high resolution mode (HR), decreases CHESS' flux by a factor of 10. Therefore, careful evaluation is needed to determine if this configuration is really needed for the CHESS science case. There are two ways to achieve the HR mode: either by adding a second smaller aperture to the M-chopper disks (3 degree), or by phasing phase the M-chopper to decrease the opening time until the desired energy resolution is reached. The former solution presents a crosstalk problem that can be efficiently evaluated with a Copley diagram [Copley 1991, 2003], while the latter can be simulated using Monte Carlo methods. We will evaluate both solutions within the coming months.

The Repetition Rate Multiplication mode has been simulated in the CHESS high flux mode for two samples: a 5 g polycrystalline graphite sample and a 1 mg single crystal sample of $K_2V_3O_8$. Shown in Figure 2-12 is the comparison of our simulations for polycrystalline graphite to a real data set collected at the SNS ARCS spectrometer at E_i = 30 meV. This simulation shows that CHESS' energy resolution matches that of ARCS very well; the phonon dispersion looks clean and without artifacts coming from the spherical detector configuration. However, the simulation also highlights the power of RRM: while ARCS can only measure the sample using one incident energy per time, CHESS can employ 5 incident energies in one measurement with increasing resolution. This will make measurements faster and more efficient. The same conclusion is also valid for the single crystal simulation, where in one measurement, CHESS can analyze the main spin wave dispersion at E_i = 5.1 meV and the 81 μeV gap at (100).

These results confirm that our guide and chopper optimizations support the science case for this spectrometer outlined in Section 1.

The simulations have been reduced and analyzed with the Mantid software [Arnold 2014], following the same reduction procedure currently used at instruments at SNS. Future upgrades to the software package will allow CHESS to merge all the RRM energies into a single file and use super-resolution techniques [Lin 2022] for this analysis.

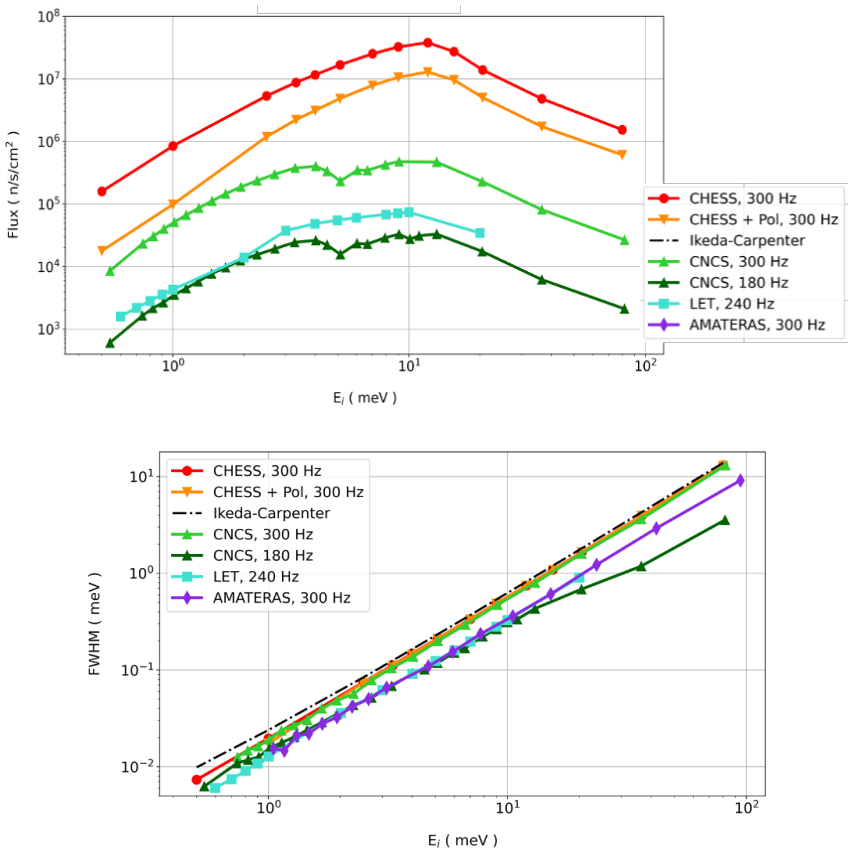

Figure 2-11 Preliminary comparison of the simulated energy resolution at the elastic line and flux for the CHESS instrument. The simulations have been performed with the MCViNE software package. The comparison is made with real data collected at CNCS, LET and AMATERAS for common mode of operations of these instruments.

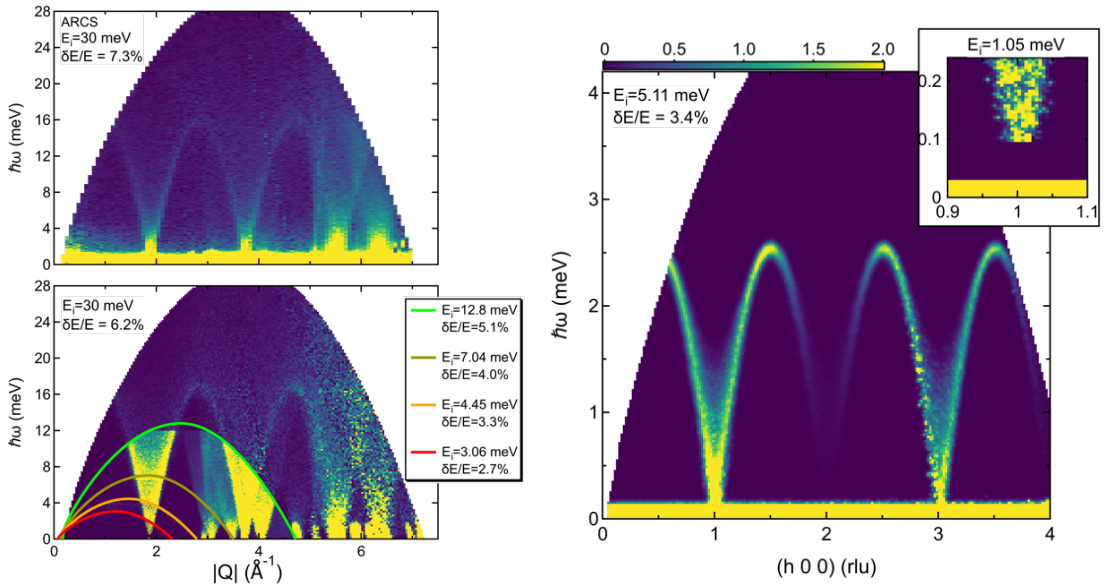

Figure 2-12 Experiment simulations using the Repetition Rate Multiplication mode for: Polycrystalline graphite at Ei=30 meV compared with the real data set collected at ARCS (left), and single crystal K2V3O8 at Ei=5.11 meV (right).

2.7 SHUTTER (WBS S.04.04.06)

For the instrument to operate in safe conditions a shutter is located right outside the wall of the bunker at 10.5 m. When closed, the operations shutter allows safe access to instrument for beamline staff operations (*e.g.*, changing samples, inspecting choppers downstream from the bunker wall, entering the detector vessel, entering the upstream cave).

2.8 MOTION SYSTEMS (WBS S.04.04.06)

The CHESS beamline will be equipped with a series of motion devices to assist users in their experiments:

- The shutter will rotate between open and closed position.
- The V-channel polarizer will rotate in/out of the beam.
- A set of circular slits will move to adjust the beam width.
- A 3000 lb crane will be used to move the sample environment in/out of the sample pit.
- A 3000 lb elevator will be employed to move the sample environment across the mezzanine to any of the three floors of the instrument.

2.9 DETECTOR VESSEL (WBS S.04.04.07)

The CHESS detector vessel will be built to house the entire detector system in vacuum (>10^{-5} torr). The current layout, shown in Figure 2-13 consists of cylindrical vessel (∅ = 6.8 m, height = 7.3 m) including the Stainless Steel (SS) ribbing skeleton. provisions were made for Vacuum ports and Electrical ports, embedded in the ribbing, and space was reserved for sample environment utilities. The intra-spaces in the ribbing will also be used to hide cables and pipelines. An airtight hatch at the back will allow access to the tank and the detectors. Sample environment will be flange mount based and bolted to the ∅ = 1.1 m sample pit, before applying vacuum. Sample environment will share the vacuum with the detector vessel. Therefore, a thimble will be mounted to create a boundary between the detector tank and the sample environment for bottom loading sample environment. This will allow beamline personnel and SE technicians to change samples without breaking the vacuum.
Finally, the guide system will be connected to the vessel by an Al or sapphire window, based on background analysis.

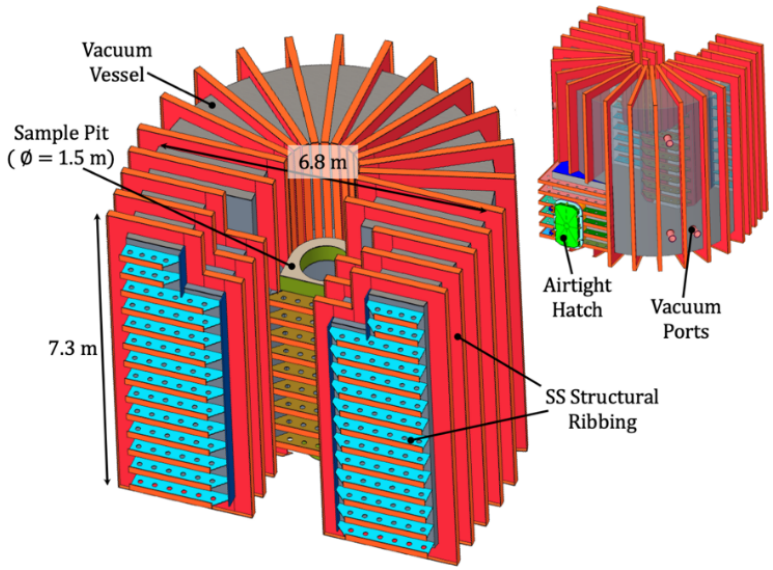

Figure 2-13 Layout of the CHESS Detector Vacuum Vessel, with its main components and dimensions.

2.10 INSTRUMENT SPECIFIC SUPPORT EQUIPMENT (WBS S.04.04.07)

2.10.1 FEA Analysis of the Detector Frame

The detector frame is responsible for supporting and keeping the CHESS detectors within reasonable deflection parameters due to gravity, avoiding pixel misalignment and changes in the instrument resolution. The frame material is chosen to avoid remnant magnetization that will interfere with the polarization mode of operation; thus, we are currently evaluating Al 6061 or Stainless-Steel SS 304 as main alloys.
The FEA analysis performed assuming a cylindrical configuration hosting 159 standard ^{3}He 8-pack detectors (50 lb. each) showed that gravity will deflect the structure along the vertical y-axis by 0.895(0.746) mm for Al 6061, and by 0.453(0.328) mm for SS 304 respectively. Figure 2-14 shows a projection of the FEA analysis for the two configurations.
Considering the different cost of the frames, engineering best practices and the implications related to the stray fields, the final selection will be made during the final design phase of the project.

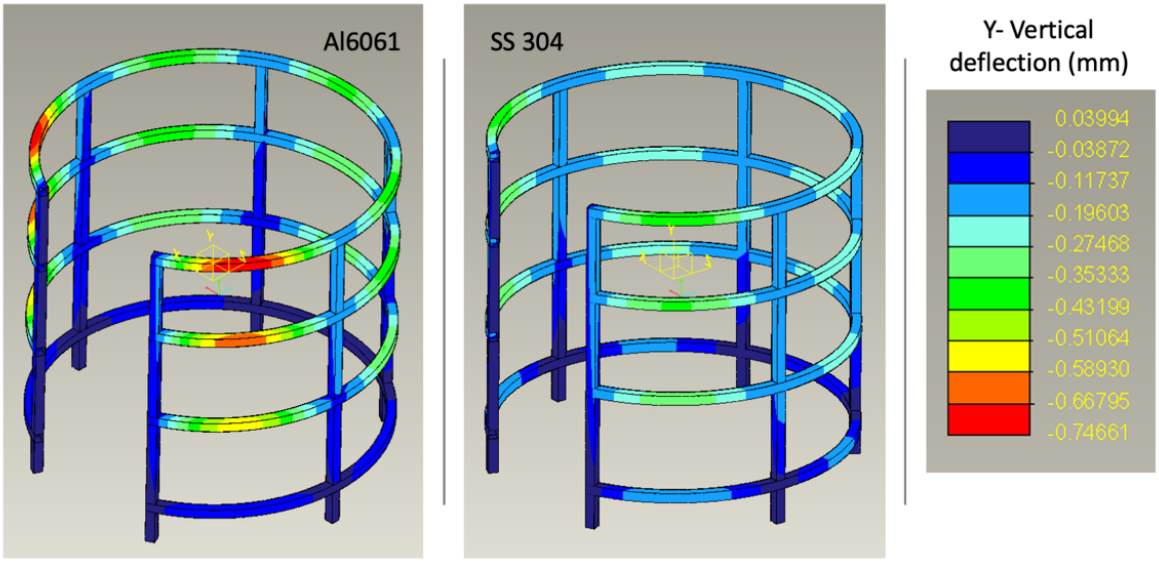

Figure 2-14 FEA Analysis of the CHESS detector frame for cylindrical configurations. This analysis was performed assuming 50 lb. detectors, supported by 1/4" tubes in Al6061 or SS304. The deflection of the spherical(cylindrical) frame along the vertical y-axis is 0.895(0.746) mm for Al 6061, and by 0.453(0.328) mm for SS 304 respectively.

2.10.2 Crane

The CHESS instrument will be equipped with a dedicated 3000 lb. bridge crane designed to cover the entire third floor above the upstream cave and detector vessel area. The crane will be used for material lifting operations (sample environment, vacuum pumps, choppers etc.) substituting, whenever possible, the STS main 30-ton crane. The CHESS bridge crane provides enough vertical height to lift the largest STS standard sample environments to load to sample position, while ensuring to stay well below the main building's 30-ton crane. ORNL staff will be trained to operate this device, and planned maintenance will be scheduled to meet safety requirements.

2.10.3 Elevator

The CHESS instrument must be able to move sample environment, racks, and materials across the three floors of the instrument independently from the rest of the STS operations. For this reason, CHESS will employ a dedicated 3000 lb. elevator to move materials (sample environment, vacuum pumps, racks etc.) from the mezzanine to any of the three floors of the instrument. This elevator substitutes the main 30 ton crane of the STS 50 m instrument building, which could be used only to move materials from the STS floor level to the third floor of the CHESS instrument.

2.11 SAMPLE ENVIRONMENTS (WBS S.04.04.08)

The CHESS beamline is expected to employ a wide range of sample environments to successfully cover its science mission, including:

- A bottom loading CCR with low background ($5 < T < 800$ K).
- An Orange Cryostat ($1.7 < T < 323$ K) with the possibility to use ^{3}He or dilution refrigerator inserts.
- A ^{3}He insert ($0.3 < T < 10$ K).
- A Dilution refrigerator insert ($0.03 < T < 1$ K).
- A compensated low background vertical field Cryo-magnet (8+ Tesla, $1.7 < T < 400$ K) with the possibility to use ^{3}He or dilution refrigerator inserts.
- A non-compensated low background vertical field Cryo-magnet (18 Tesla, $1.7 < T < 400$ K) with the possibility to use ^{3}He or dilution refrigerator inserts.
- A horizontal field magnet (5+ Tesla)
- A furnace with a niobium or vanadium shield, and with option for quartz gas flow insert for high temperature experiments ($300 < T < 1900$ K).
- A high temperature neutron electrostatic levitator (NESL) for high temperature experiments ($300 < T < 3000$ K).

The CHESS sample environment interface will follow design guidelines provided by STS sample environment standardization effort to maximize usage of sample environments across STS instruments. The STS sample environment standardization guidelines provide recommendations for flange dimensions, bolt patterns, keep out zones, etc. By following STS sample environment standards, sample environments designed for CHESS will be able to be used at other STS instruments and vice-versa.

2.12 INSTRUMENT INFRASTRUCTURE (WBS S.04.04.09)

The following is a list of infrastructures needed to operate the CHESS beamline.

2.12.1 Vacuum Systems

Standard STS dry pump systems will provide vacuum for the 5 choppers (10^{-5} torr), while the shared vacuum system in the bunker serves the guide system (10^{-3} torr). Three emergency dry pumps will be attached to the guide system in case of a sudden loss of vacuum in the bunker system.
The Detector tank will have its own dedicated redundant vacuum system made of a total set of 8 turbo pumps, 8 dry pumps, 4 polycolds and 2 rough pumps that will maintain a pressure of 10^{-5}-10^{-6} torr to allow user experiments. The pumps will be distributed on the first and second floor of the instrument to maximize the efficiency of the system. Exhaust from the vacuum pumps will be vented to atmosphere via HEPA filters.

2.12.2 Sensible Chilled Water System

The eight turbo pumps, the compressor and few sample environment will employ sensible chilled water to cool down, eliminating the excess heat. The pipeline will be routed to cover all the three floors of the CHESS beamline with easy access points for sample environment and turbo pumps.

2.12.3 Process Water (PW)

CHESS has no planned loads for this system.

2.12.4 Compressed Air (CA)

The CHESS beamline will have a pipeline dedicated to compressed air, this will used in conjunction with sample environment to dry samples and clean surfaces.

2.12.5 Cryogens

Liquid Nitrogen N_2 and liquid ^4He will be needed to cool down samples in conjunction with different sample environments. CHESS will have a designated area to safely store N_2 and ^4He gas cylinders as well as a provision for a ^4He recovery system.

2.12.6 Fire Protection

Specific needs will be identified by an evaluation by the Fire Protection Engineer. CHESS is expected to need sprinkler heads on the second floor (control hutch), the first floor (utility room) and on the upstream cave. In addition, smoke detectors are required in these areas as well.

2.12.7 Global Controls

ICS will provide connections to the new STS timing system.

2.12.8 Remote Operations

TBD.

2.12.9 Power and HVAC

CHESS will provide five 480VAC welding units, typically used at SNS, at the beamline close to the instrumentation. We will make provisions to increase the size of few panels to 100 A, to avoid overload when Cryo-magnets are attached. Instrument loads are currently being evaluated with our electrical engineers and they will be specified in the final design phase.

2.12.10 Utility Drops

In addition to the utilities described above, a full complement of standard STS Target Building utility drops will be installed across the instrument. These are intended for general use as well as sample environment use and consist of:

- Compressed air (CA).
- Gaseous Nitrogen (N_2).
- Gaseous Helium (^4He).
- Sensible chilled water supply and return (CWS&R).
- 3000 lb bridge crane.

- 3000 lb material elevator.
- ^{4}He recovery system.
- He-Glove box for non-radioactive sample storage.
- Electrical panels for sample environment (including motion panels).
- Electrical panel for polarization coils.

2.13 CHESS INSTRUMENT CONTROLS AND DAQ (WBS S.06.04.04)

Instrument Control System (ICS) shall meet the requirements in *S06040200-SR0001*, *Integrated Control Systems Instruments Control and Data Acquisition Requirements Document*. ICS will provide the following systems:

- DAQ.
- Network.
- Racks.
- Wiring.
- Timing System.
- STS standard Personnel Protection System and Oxygen Deficiency Hazard equipment.

2.14 SCIENTIFIC SOFTWARE (WBS S.04.02)

The Scientific Software shall include programs and procedures to operate safely and efficiently within the context of the user program. A new software package for data reduction, analysis and visualization will be considered during the preliminary design phase of the project.

3. BIBLIOGRAPHY

Albrecht, T, et al. 1997. "First observation of ferromagnetism and ferromagnetic domains in a liquid metal." *Applied Physics A: Materials Science & Processing* **65**, no. 2, 215-220.

Anunciado, D. B., V. P. Nyugen, G. B. Hurst, et al. 2017. "In vivo protein dynamics on the nanometer length scale and nanosecond time scale," *J. Phys. Chem. Lett.* **8**(8), 1899–1904.

O. Arnold, J. Bilheux, J. Borreguero, et al., 2014 "Mantid—data analysis and visualization package for neutron scattering and μSR experiments," *Nuclear Instruments and Methods in Physics Research Section A: Accelerators, Spectrometers, Detectors and Associated Equipment*, vol. **764**, pp. 156–166.

Balz, C., B. Lake, J. Reuther, et al. 2016. "Physical realization of a quantum spin liquid based on a complex frustration mechanism," *Nat. Phys.* **12**, 942–949.

Bewley R. I. et al. 2011. "LET, a cold neutron multi-disk chopper spectrometer at ISIS." *Nucl. Instrum. Meth. Phys. Res. A,* **637**, 128-134.

Bewley R. I., Taylor J. W., and Bennington S. M. 2011, "Let: A low energy multiple chopper spectrometer at ISIS." Notiziario Neutroni e Luce di Sincrotrone, **16**, no. 2, pp. 4-13.

Bigault, T. G. Delphin, A. Vittoz, V. Gaignon, and P. Courtois 2014. "Recent polarizing supermirror projects at the ILL." In Journal of Physics: Conference Series, vol. 528, no. 1, p. 012017. IOP Publishing.

Burankova, T., R. Hempelmann, A. Wildes, et al. 2014. "Collective ion diffusion and localized single particle dynamics in pyridinium-based ionic liquids," *J. Phys. Chemistry B* **118**(49), 14452-60.

Carpenter J. M., D. L. Price, and N. J. Swanson 1978, "IPNS - a national facility for condensed matter research," *Report ANL*, vol. **78-88**, p. 291.

Chandler 2017. "From 50 years ago, the birth of modern liquid-state science." *Ann. Rev. Phys. Chem.* **68**, 19-38. https://doi.org/10.1146/annurev-physchem-052516-044941

Copley J. R. 1991, "Transmission properties of a counter-rotating pair of disk choppers," *Nuclear Instruments and Methods in Physics Research,* **303**, pp. 332–341.

Copley J. R. 2003, "An acceptance diagram analysis of the contaminant pulse removal problem with direct geometry neutron chopper spectrometers," *Nuclear Instruments and Methods in Physics Research, Section A: Accelerators, Spectrometers, Detectors and Associated Equipment,* **510**, pp. 318–324, 9.

Delaire, O., J. Ma, K. Marty, et al. 2015. "Giant anharmonic phonon scattering in PbTe," *Nat. Mater.* **10**(8), 614.

Ding J., Niedziela J. L., D. Bansal, J. Wang, X. He, A. F. May, G. Ehlers, D. L. Abernathy, A. Said, A. Alatas, Y. Ren, G. Arya, and O. Delaire, 2020 "Anharmonic lattice dynamics and superionic transition in $AgCrSe_2$", *PNAS* **117**(8) 3930-3937.

Disch S. et al. 2014. "Spin excitations in cubic magnemite nanoparticles studied by time-of-flight neutron spectroscopy." *Physical Review B* **89**(6), 064402.

DOE (US Department of Energy). 2016. *Basic Research Needs Workshop on Quantum Materials for Energy Relevant Technology*, February 8–10, 2016, BES Workshop Reports, Office of Basic Energy Sciences.

DOE Energy Innovation Hub https://www.jcesr.org/

Doster, W., S. Cusack, and W. Petry. 1989. "Dynamical transition of myoglobin revealed by inelastic neutron scattering," *Nature* **337**(6209), 754–56.

Ehlers, G., G. Sala, F. Gallmeier, et al. 2018. "Figure-of-merit for a cold coupled moderator at the SNS Second Target Station suited for direct geometry inelastic spectrometers," *J. Phys.: Conf. Ser.* **1021**, 012032.

Frick, B., and D. Richter. 1995. "Microscopic basis of the glass transition in polymers from neutron scattering studies," *Science* **267**(5206), 1939–45.

Fritsch, V. N. Bagrets, G. Goll, et al. 2014. "Approaching quantum criticality in a partially geometrically frustrated heavy-fermion metal," *Phys. Rev. B* **89**(5), 054416.

Gaspar, A. M., S. Busch, M.-S. Appavou, et al. 2010 "Using polarization analysis to separate the coherent and incoherent scattering from protein samples," *Biochim. Biophys. Acta* **1804**(1), 76–82.

Hafner, J. C. E, A, T. Kluyver, M. Bertelsen, M. U. Kahaly, Z. Lecz, S. Nourbakhsh, A. P. Mancuso, and C. Fortmann-Grote 2020 "VINYL: The VIrtual Neutron and x-raY Laboratory and its applications," *Advances in Computational Methods for X-Ray Optics V* (O. Chubar and K. Sawhney, eds.), vol. **11493**, pp. 190-200, International Society for Optics and Photonics, SPIE.

Iyad I. Al-Quasir, Campbell A. A., Sala G., Lin J. Y. Y., Yongqiang Cheng, Islam F. F. Abernathy D. L. and Stone M. B. 2020. "Vacancy-driven variations in the phonon density of states of fast neutron irradiated nuclear graphite." *Carbon* **168**, 42-54.

Jaiswal A., Egami T., Kelton K. F., Schweizer K. S. and Zhang Y. 2016. "Correlation between fragility and the Arrhenius crossover phenomenon in metallic, molecular and network liquids." *Phys. Rev. Lett.* **117**, 205701.

Kamiya, Y. and Batista C. D. 2014. "Magnetic vortex crystals in frustrated Mott insulator," *Phys. Rev. X* **4**, 011023.

Ke Yang, Zhikun Cai, Abhishek J., Madhusudan T., Moore S. J. and Zhang Y. 2016. "Dynamic odd-even effect in liquid *n*-alkanes near their melting points." *Ange. Chem.,* **55**(45), 14090-14095.

Kikuchi T., Nakajima K., Ohira-Kawamura S. et at. 2019. "Background issues encountered by cold neutron chopper spectrometer AMATERAS.", *Physica B: Condensed Matter*, **564**, 45-53.

Lanigan-Atkins T., S. Yang*, J. L. Niedziela, D. Bansal, A. F. May, A. A. Puretzky, J.Y.Y. Lin, D. Pajerowski, T. Hong, S. Chi, G. Ehlers, and O.Delaire 2020. "Extended anharmonic collapse of phonon dispersions in SnS and SnSe", *Nature Communications* **11**(1), 1-9.

Lee, P. A., N. Nagaosa, and X.-G. Wen. 2006. "Doping a Mott insulator: Physics of high-temperature superconductivity," *Rev. Mod. Phys.* **78**(1), 17–85.

Leonov, A. O., and M. Mostovoy. 2015. “Multiply periodic states and isolated skyrmions in an anisotropic frustrated magnet,” *Nat. Commun*, **6**, 8275.

Li C. W., J. Hong, A. F. May, et al. 2015. “Orbitally driven giant phonon anharmonicity in SnSe,” *Nat. Phys.* **11**, 1063.

Li Min, Rhodes Z. et al. 2020. “Recent advancements in rational design of non-aqueous organic redox flow batteries.” *Sustainable Energy and Fuels* **4**, 4370-4389.

Li Zhixia, Robertson L. A. et al. 2020. “Realistic ion dynamics through charge renormalization in non-aqueous electrolytes.” *J. Phys. Chem. B* **124**(15), 3214-3220.

Lin, Jiao YY, Hillary L. Smith, Garrett E. Granroth, Douglas L. Abernathy, Mark D. Lumsden, Barry Winn, Adam A. Aczel, Michael Aivazis, and Brent Fultz 2016. "MCViNE–An object-oriented Monte Carlo neutron ray tracing simulation package." *Nuclear Instruments and Methods in Physics Research Section A: Accelerators, Spectrometers, Detectors and Associated Equipment* **810**, 86-99.

Lin, Jiao Y. Y., Fahima Islam, Gabriele Sala, Ian Lumsden, Hillary Smith, Mathieu Doucet, Matthew B. Stone et al. 2019. "Recent developments of MCViNE and its applications at SNS." *Journal of Physics Communications* **3**, no. 8, 085005.

Lin, Jiao Y. Y., G. Sala, and M. B. Stone 2022, “A super-resolution technique to analyze single-crystal inelastic neutron scattering measurements using direct-geometry chopper spectrometers,” *Review of Scientific Instruments*, **93**, no. 2, p. 025101.

Loong C. K., Ikeda S. and Carpenter J. M., 1987. “The resolution function of a pulsed-source neutron chopper spectrometer.” *Nucl. Instrum. Meth. Phys. Res. A* **260**(2-3), 381-402.

Lumsden M. D., S. E. Nagler, B. C. Sales, D. A. Tennant, D. F. McMorrow, S.-H. Lee, and S. Park 2006. “Magnetic excitation spectrum of the square lattice S=1/2 Heisenberg antiferromagnet $K_2V_3O_8$.” *Phys. Rev. B* **74**, 214424.

Luo P., Zhai Y., Senses E., Mamontov E., Xu G. and Faraone A. 2020. “Influence of Kosmotrope and Chaotrope salts on water structural relaxation.” *J. Phys. Chem. Lett.* **11**, 8970-8975.

Mamontov E., Y. Cheng, L. Daemen, A. I. Kolesnikov, A. J. Ramierz-Cuesta, M. R. Ryder, and M. B. Stone, 2020. “Hydration-induced disorder lowers the energy barriers for methyl rotation in drug molecules.” Journal of Physical Chemistry Letters **11**, 10256.

Mamontov E., Y. Cheng, L. Daemen, J. Keum, A. Kolesnikov, D. Pajerowski, A. Podlesnyak, A. Ramirez-Cuesta, M. Ryder, and M. B. Stone, 2020. “Effect of hydration on the molecular dynamics of hydroxychloroquine sulfate.” ACS Omega **5**, 21231.

Martin, I., and C. D. Batista. 2008. “Itinerant electron-driven chiral magnetic ordering and spontaneous quantum Hall effect in triangular lattice models,” *Phys. Rev. Lett.* **101**(15), 156402.

Manley M. E., Hellman O., Shulumba N., May A. F., Stonaha P. J., Lynn J. W., Garlea V. O., et al. 2019 “Intrinsic anharmonic localization in thermoelectric PbSe,” *Nature Comm.* **10**, 1928.

Mauro, N. A., A. J. Vogt, K. S. Derendorf, M. L. Johnson, G. E. Rustan, D. G. Quirinale, A. Kreyssig et al. 2016. "Electrostatic levitation facility optimized for neutron diffraction studies of high temperature liquids at a spallation neutron source." *Review of Scientific Instruments* **87**, no. 1, 013904.

Meyer, Andreas, Sebastian Stüber, Dirk Holland-Moritz, Oliver Heinen, and Tobias Unruh 2008. "Determination of self-diffusion coefficients by quasi-elastic neutron scattering measurements of levitated Ni droplets." *Physical Review B* **77**, no. 9, 092201.

Minnich, A. J., M. S. Dresselhaus, Z. F. Ren, et al. 2009. "Bulk nanostructured thermoelectric-materials : Current research and future prospects," *Energy Environ. Sci.* **2**, 466.

Mühlbauer, S., B. Binz, F. Jonietz, et al. 2009. "Skyrmion lattice in a chiral magnet," *Science* **323**(5916), 915–919.

Newville M., T. Stensitzki, D. B. Allen, and A. Ingargiola, "LMFIT: Non-Linear Least-Square Minimization and Curve-Fitting for Python," Sept. 2014.

Nickels, J. D., H. O'Neill, L. Hong, et al. 2012. "Dynamics of protein and its hydration water: Neutron scattering studies on fully deuterated GFP," *Biophys. J*, **103**, 1566.

Nickels, J. D., S. Perticaroli, H. O'Neill, et al. 2013. "Coherent neutron scattering and collective dynamics in the protein, GFP," *Biophys. J.* **105**, 2182.

Nickels, J. D., S. Chatterjee, C. B. Stanley, et al. 2017. "The in vivo structure of biological membranes and evidence for lipid domains," *PLoS Biol*, **15**, e2002214.

Niedziela J. L., Bansal D., A. F. May, J. Ding, T. Lanigan-Atkins, G. Ehlers, D. L. Abernathy, A. Said & O. Delaire, 2019 "Selective Breakdown of Phonon Quasiparticles across Superionic Transition in CuCrSe2", *Nature Physics*, **15**, 73-78.

Nilsen G. J., et al. 2017. "Polarisation on the LET time-of-flight spectrometer." *J. Phys.: Conf. Ser.* **862**, 012019.

Okawa, M., M. Matsunami, K. Ishizaka, et al. 2010. "Strong valence fluctuation in the quantum critical heavy fermion superconductor β-YbAlB4: A hard x-ray photoemission study," *Phys. Rev. Lett.* **104**, 247201.

Orenstein, J., and A. J. Millis. 2000. "Advances in the physics of high-temperature superconductivity," *Science* **288**(5465), 468.

Paddison, J.A.M., M. Daum, Z. Dun, et al. 2017. "Continuous excitations of the triangular-lattice quantum spin liquid YbMgGaO4," *Nat. Phys*. **13**, 117.

Paulus et al. 2008. "Lattice dynamics to trigger low temperature oxygen mobility in solid oxide ion conductors." *J. Am. Chem. Soc.* **130**, 16080–16085.

Perticaroli, S., J. D. Nickels, G. Ehlers, et al. 2013. "Secondary structure and rigidity in model proteins," *Soft Matter* **9**, 9548.

Perticaroli, S., G. Ehlers, C. B. Stanley, et al. 2017. "Description of hydration water in protein (green fluorescent protein) solution," *J. Am. Chem. Soc*, **139**, 1098.

Pfleiderer, C. 2009. “Superconducting phases of ff-electron compounds,” *Rev. Mod. Phys.* **81**(4), 1551.

Reske, J., D. M. Herlach, F. Keuser, K. Maier, and D. Platzek 1995. "Evidence for the existence of long-range magnetic ordering in a liquid undercooled metal." *Physical Review Letters* **75**, no. 4, 737.

Rhodes Zayn, Cabrera-Pardo J. R., Li Min and Minteer S. D. 2020. “Electrochemical advances in non-aqueous redox flow batteries.” *Redox Flow Batteries Isr. J. Chem.*

Robertson L. A., Li Zhixia, Cao Y. et al. 2019. “Observation of micro-heterogeneity in highly concentrated non-aqueous electrolyte solutions.” *J. Am. Chem. Soc.* **141**(20), 8041-8046.

Rowley, S., Spalek, L., Smith, R. et al. 2014. Ferroelectric quantum criticality. *Nature Phys* **10,** 367–372.

Sala, G., J.Y.Y. Lin, V. B. Graves, et al. 2018. “Conceptual design of CHESS, a new direct-geometry inelastic neutron spectrometer dedicated to studying small samples,” *J. Appl. Crystallogr*, **51**, 282.

Seki S. et al. 2010. “Electromagnons in the spin collinear state of a triangular lattice antiferromagnet” Phys. Rev. Lett. **105**, 097207.

Turton, D. A., H. M. Senn, T. Harwood, et al. 2014. “Terahertz underdamped vibrational motion governs protein-ligand binding in solution,” *Nat. Commun.* **5**, 3999.

Vickery, A., and P. P. Deen. 2014. “Choppers to optimise the repetition rate multiplication technique on a direct geometry neutron chopper spectrometer,” *Rev. Sci. Instrum.* **85**, 115103.

Walter P. N., Jaiswal A., Cai. Z. and Zhang Y. 2018. “*Liquidlib:* A comprehensive toolbox for analyzing classical and *ab initio* molecular dynamics simulations of liquids and liquid-like matter with application to neutron scattering experiments.” *Comp. Phys. Comm.* **228**, 209-218.

Wang Wei, Luo Q., Li Bin, Wei X., Li Liyu and Yang Zhenguo 2012. “Recent progress in redox flow battery research and development.” *Adv. Funct. Mater.* **23**, 970-986.

Willendrup P., E. Farhi, E. Knudsen, U. Filges, and K. Lefmann 2014, “Mcstas: Past, present and future,” *Journal of Neutron Research* **17**, pp. 35–43.

Willendrup P. and Lefmann K. 2020. “McStas (i): Introduction, use, and basic principles for ray-tracing simulations”. *Journal of neutron Research* **22**, 1-16.

Wilde, G., G. P. Görler, and R. Willnecker 1996. "Specific heat capacity of undercooled magnetic melts." *Applied physics letters* **68**, no. 21, 2953-2955.

Yashima, M., S. Kawasaki, H. Mukuda, et al. 2007. “Quantum phase diagram of antiferromagnetism and superconductivity with a tetracritical point in CeRhIn5 in zero magnetic field,” *Phys. Rev. B* **76**, 020509.

Zhang J. et al. 2019. “Long-range antiferromagnetic order in a rock salt high entropy oxide.” *Chemistry of Materials* **31** (10), 3705-3711.

Zheng Y., Lu T., Polash Md M. H., Rasoulianboroujeni M., Liu N., Manley M. E., Deng Y., Sun P. J., Chen X. L., Hermann R. P., Vashaee D., Heremans J. P., Zhao H. 2019. “Paramagnon drag in high thermoelectric figure of merit Li-doped MnTe,” *Sci. Adv.* **5**, eaat9461.

4. REFERENCES

Document Number	Document Title
S04040100-SRD10000	Second Target Station Project: CHESS Instrument Requirements Document
S04040100-CMT10000	Second Target Station Project: CHESS Instrument Schematic
S04040200-DES10000	Second Target Station Project: CHESS Optics Design Description
S06040200-SR0001	Integrated Control Systems Instruments Control and Data Acquisition Requirements Document
S04000000-TRT10000	STS Project Detector Needs for STS Instruments

APPENDIX A.

APPENDIX A. ES&H EVALUATION

TBD.

APPENDIX B. MCSTAS MODEL

TBD.